Chem Soc Rev

This article was published as part of the

Conducting polymers for carbon electronics themed issue

Guest editor Professor Yung Woo Park

Please take a look at the issue 7 2010 table of contents to access other reviews in this themed issue

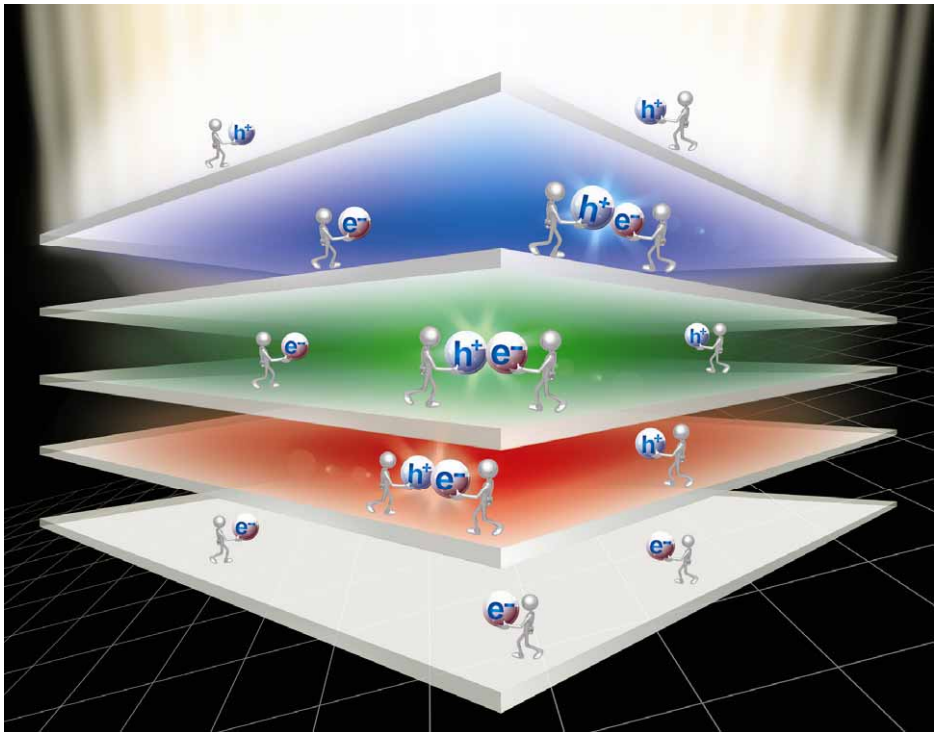

Water/alcohol soluble conjugated polymers as highly efficient electron transporting/injection layer in optoelectronic devices†

Fei Huang,* Hongbin Wu and Yong Cao*

Received 4th November 2009
First published as an Advance Article on the web 10th March 2010
DOI: 10.1039/b907991m

Water/alcohol soluble conjugated polymers (WSCPs) can be processed from water or other polar solvents, which offer good opportunities to avoid interfacial mixing upon fabrication of multilayer polymer optoelectronic devices by solution processing, and can dramatically improve charge injection from high work-function metal cathode resulting in greatly enhancement of the device performance. In this *critical review*, the authors provide a brief review of recent developments in this field, including the materials design, functional principles, and their unique applications as interface modification layer in solution-processable multilayer optoelectronic devices (135 references).

1. Introduction

Conjugated polymers (CPs) have attracted considerable attention in past decades due to their significant application potential in organic electronic devices (such as polymer light-emitting diodes (PLEDs),[1,2] polymer solar cells (PSCs)[3–5] and organic filed effect transistors (OFETs)[6,7] and chemo-/bio-sensors.[8–10] Their π-conjugated main chains offer them a delocalized electronic structure which endow them unique optoelectronic properties different from traditional polymers. CPs can be processed by spin-coating or ink-jet printing technique *via* solution processing, while small molecular organic semiconductors are usually processed by high vacuum vapor deposition.[1,11] Thereby, compared to the small molecule organic devices, CPs based organic electronic devices (such as PLEDs, PSCs) will potentially combine the advantages of ease of fabrication and lower production cost, especially for the large-size devices. However, the solution process also brings a big challenge for fabricating organic electronic devices compared to the small molecular organic semiconductors. Now it is well known that most of organic electronic devices need a multilayer device structure to ensure a better performance. One of the typical examples is organic light-emitting diodes (OLEDs) that usually use a hole transporting/injection layer (HTL) and an electron transporting/injection layer (ETL) to facile hole and electron injection/transport from anode and cathode, respectively, to maximize the device performance, resulting in a generally used multilayer device structure: indium tin oxide (ITO) anode/HTL/emissive layer (EML)/ETL/metallic electrode cathode (Fig. 1).[12–15] For small molecular organic semiconductors, it is easy to realize the multilayer device structure through high vacuum vapor deposition. For CPs based PLEDs, it is very challengeable to realize the multilayer device structure by solution process. Since most of

Institute of Polymer Optoelectronic Materials and Devices, Key Lab of Specially Functional Materials of the Ministry of Education, South China University of Technology, Guangzhou 510640, P. R. China. E-mail: msfhuang@scut.edu.cn, poycao@scut.edu.cn
† Part of the Conducting Polymers for Carbon Electronics themed issue.

Fei Huang

Fei Huang received his BS degree in Chemistry from Peking University in 2000 and gained his PhD degree in Materials Science from the South China University of Technology in 2005 under the supervision of Prof. Yong Cao. After postdoctoral work at University of Washington with Prof. Alex K.-Y. Jen, he began his academic career in 2009 as a professor of South China University of Technology. His main interests are in the fields of organic functional materials and devices for opto-electronics.

Hongbin Wu

Hongbin Wu received a PhD in materials physics from the South China University of Technology in 2006 and joined the University as a research fellow at the same year and later was promoted as associate professor in 2008. His current research interests are polymer optoelectronic devices including light-emitting devices and solar cells.

the commonly used emissive and transport materials have similar solubility in common organic solvents, this may cause erosion of the subsequent layers during multilayer integration. Many efforts have been performed to overcome this problem. For example, crosslinkable HTL and EML materials have been developed a nd these materials can form robust films with excellent solvent resistance after thermo- or photo-crosslinking.[14,16,17] Another approach is to develop new conjugated polymers with totally orthogonal solubility with the commonly used transporting/injection or active materials.[18–20] Since most of the commonly used conjugated polymer active materials, such as poly[2-methoxy,5-(2-ethylhexyloxy)-1,4-phenylenevinylene] (MEH-PPV), poly[2-(4-(3′,7′-dimethyloctyloxy)-phenyl)-*p*-phenylenevinylene) (*P*-PPV), poly(3-hexylthiophene) (P3HT) *etc*., do not dissolve in high polar solvents, water/alcohol soluble conjugated polymers (WSCPs), which usually have good solubility in high polar solvents, are good candidates for the fabrication of multilayer devices with those traditional conjugated polymers. This has been proved by recent research results that the interface mixing of different polymer layers can be successfully avoided in the bilayer polymer structure spun cast from solvents with different polarity, while spin coating both polymer layers from similar polarity solvents resulted in severe mixing of the two polymer layers and dissolution of the underlying layer.[21,22] Besides, there are many other advantages of WSCPs for application in organic electronic devices. Firstly, WSCPs can be processed from environmental-friendly solvents (such as alcohol and water), which is more favorable in future industry applications. Secondly, most of WSCPs are conjugated polyelectrolytes with charged pendant groups on their side chains. Thus, the layer by layer self-assembling (LBL) technique of polyelectrolytes[23] can be used for WSCPs to fabricate organic electronic devices.[24] Most importantly, it was recently found that the WSCPs with polar pendant groups can also dramatically improve charge injection from metallic electrodes into organic active layers resulting in significant enhancement in the device performance.[18] Due to these advantages, more and more efforts have been put in this area and significant progresses have been made in recent years. This review presents recent developments of WSCPs, including not only conjugated polyelectrolytes but also those neutral WSCPs, and their application in organic electronics devices, especially as the interfacial modification layers in organic electronics devices. It should be noted that conjugated polyelectrolytes have been developed rapidly in recent years due to their successful application in biological and chemical sensors and there are several good reviews about the synthesis and applications of these polymers in sensors and related optoelectronic devices.[8–10,18–20] The reader is encouraged to consult these reviews for different perspectives in this field.

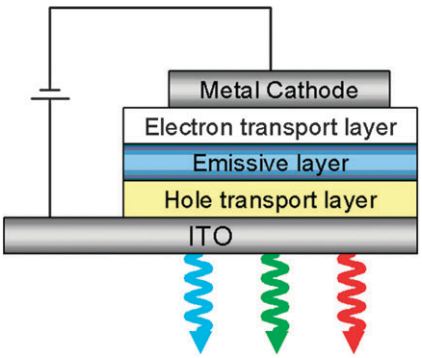

Fig. 1 Schematic drawing of typical multilayer OLEDs' device structure.

2. The development of WSCPs for PLEDs

WSCPs have been developed as early as the mid 1980s and the researches were originally focused on the "self-doped" conductive polymers.[25–27] Later on, it was found that WSCPs can be used as highly sensitive materials in chemo-/bio-sensors due to their good water solubility (applications to biological systems) and unique "amplification property" of conjugated polymers.[8–10] The successful application of WSCPs in chemo-/bio-sensors has led to the significant progress on the development of new synthetic protocols for novel WSCPs with various structures. The most straightforward way to develop WSCPs is to simply introduce the water-soluble polar groups (such as ammonium groups, sulfonate groups, phosphonate groups *etc*.) into those traditional conjugated polymers. In the meantime, many efforts have been put on the application of WSCPs in organic electronic devices, especially for PLEDs, due to their many obvious advantages discussed above. Cimrová *et al*.[28] reported the PLEDs based on a sulfonated poly(*p*-phenylene) (PPP) **P1** (Scheme 1). It was found that **P1**'s conductivity is highly depend on its counter ions (H^+, Na^+ or $N^+C_{14}H_{29}(CH_3)_3$). Preliminary dielectric spectroscopy data indicated that the room temperature conductivity (at 10^{-1} Hz) of **P1** decreased from 7×10^{-12} S cm^{-1} to 4×10^{-14} S cm^{-1} when Na^+ was replaced by the larger $N^+C_{14}H_{29}(CH_3)_3$ ion. When **P1** was used in single layer PLEDs with configuration: ITO/**P1**/Al, the devices' electroluminescence (EL) spectra were significantly influenced by the counterions of **P1**. Device based on **P1** with Na^+ counterion exhibited EL emission at 413 nm, while devices' EL emission were red shifted to 454 nm for device based on **P1** with H^+ counterion and 480–500 nm for device based on **P1** with $N^+C_{14}H_{29}(CH_3)_3$ counterion, respectively. The external quantum efficiencies (EQEs) of **P1**-based PLEDs were in the range of 0.5–0.8% with counterions H^+ or Na^+. Similar counterions effect on WSCPs based PLEDs were

Yong Cao

Yong Cao, physical chemist, Professor of South China University of Technology since 1999. BS from Department of Chemistry, Leningrad (now San Petersburg) University, PhD degree from Tokyo University, Japan. He was visiting senior researcher at University of California, Santa Barbara in 1988–1990 and senior scientist of UNIAX Corporation in 1990–1998. Current research interest: Polymer optoelectronic materials and devices.

also reported by Thünemann *et al.*[29,30] A poly(1,4-phenyleneethynylene carboxylate) **P2** with various cationic counterions were developed and used as EML in PLEDs with configuration ITO/**P2**/Al. The peak wavelength of the electroluminescence shifts from 430 to 515 nm for single-layer LEDs when the counterions were changed from tetraethylammonium to sulfonium ions. No efficiency data was reported in these reports. Besides, many efforts have been performed on using LBL technique to fabricate WSCPs based PLEDs.[31–34] By using LBL technique, the thickness of polymer active layers can be precisely controlled on the molecular level and their surface morphologies can be well optimized. One typical example was reported by Baur *et al.*[34] that PLEDs with the configuration: ITO/[**P3**/**P4**]$_n$/Al were fabricated by using layer-by-layer self-assembly of cationic and anionic PPP derivatives **P3** and **P4** as the active layer. For comparison, the PLEDs based on the layer-by-layer self-assembled EML of **P3** and several non-conjugated polycations were also fabricated. Among them, devices based on **P3**/**P4** layer-by-layer self-assembled exhibited the best device performance, showing a relative low turn-on voltage (7 V) and improved EQE of 0.002%. Despite the many attracting advantages of WSCPs for application in PLEDs, the performance of WSCPs based PLEDs reported in this period were usually very poor. One possible reason for the poor performance of WSCPs based PLEDs is the strong interchain interaction of them due to the existence of polar or ionic side group. Very recently, the time-resolved optical spectroscopy research results on WSCPs revealed that the luminescence of WSCPs can be severely quenched by the ions incorporated in films due to the formation of charge-transfer states that are stabilized by the Coulomb field of ions.[35] Therefore, despite numerous efforts, high-efficiency PLEDs with good color purity based on WSCPs remains a great challenge these days.

In 2004, we reported that the polar pendant groups of WSCPs can dramatically improve charge injection from high work-function metallic electrodes into organic active layers to greatly improve the device performance.[36,37] Thus, high-efficiency PLEDs can be realized by using WSCPs as interfacial modification layers and this can offer many opportunities for realizing PLEDs with new device structures. Since then, more and more research groups involved in this area and many state of the art PLEDs based on WSCPs interfacial modification materials have been reported.

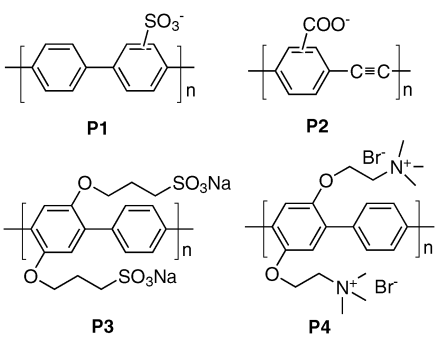

Scheme 1 Molecular structures of **P1–P4**.

2.1 Amino- and ammonium-functionalized WSCPs

In 2004, we reported the first PLEDs based on amino-/ammonium-functionalized polyfluorene WSCPs **P5–P8** (Scheme 2).[36] Two kinds of amino-functionalized polyfluorene CPs **P5** and **P6** were obtained by Suzuki coupling of amino-functionalized dibromofluorene monomer and 2,7-bis(4,4,5,5-tetramethyl-1,3,2-dioxaborolan-2-yl)-9,9-dioctylfluorene for **P5** or 1,4-benzene diboronic acid for **P6**, respectively. The corresponding polyelectrolytes **P7** and **P8** were prepared by a quaternization treatment of their precursor polymer with bromoethane. All the polymers have similar photophysical properties as those traditional polyfluorene homopolymers and exhibited strong blue emission both in solution and in thin solid films. The optical band gaps of them were at around 2.9 eV, which is determined from their absorption onset. The electrochemical studies indicated that their highest occupied molecular orbital (HOMO) levels are at around −5.6 eV to −5.7 eV and their LUMO levels are at around −2.1 eV to −2.2 eV. **P7** and **P8** have good solubility in high polar solvents such as methanol, dimethylformamide (DMF), dimethyl sulfoxide (DMSO) *etc*., due to the polar ammonium groups on their side chains. **P5** and **P6** are soluble in common non-polar organic solvents such as toluene, chloroform *etc*. In most of case, amino-functionalized CPs are insoluble in high polar solvents (such as alcohol and water) by themselves and they are usually made as the precursor polymers to further obtain ammonium-functionalized conjugated polyelectrolytes through a quaternization treatment.[8] However, it was found that these amino-functionalized CPs can be dissolved in high polar solvents under the presence of small amount of acetic acid due to a weak interaction between the nitrogen atoms in amino groups of the side chain and the acetic acid.[38] Most interestingly, the infrared spectroscopy (IR) research results on the conjugated polymer films spun cast from methanol/acetic acid mixed solvents indicate that the added acetic acid could be completely removed from the polymers after dried in a vacuum.[39] Thereby, these amino-functionalized WSCPs can combine the advantages of those traditional neutral CPs and conjugated polyelectrolytes, which can be processed from environmental-friendly solvents (such as water and alcohol) and can avoid the negative effect of the counterions among

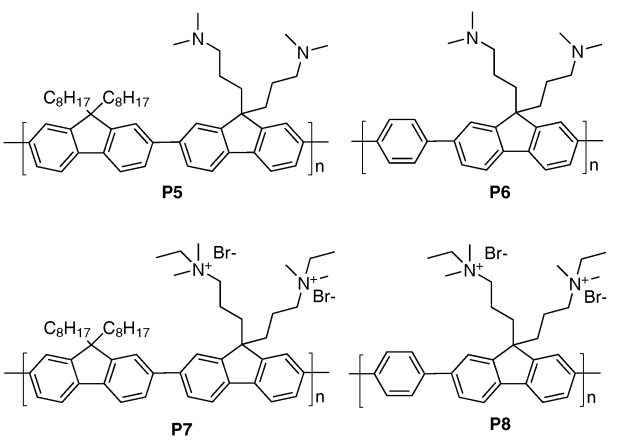

Scheme 2 Molecular structures of **P5–P8**.

those conjugated polyelectrolytes. Since the synthetic protocol of the amino-/ammonium-functionalized WSCPs have been developed very well,[8,18] both of them have been intensively investigated for organic electronic device application. In addition, since the ammonium-functionalized WSCPs are originated from the amino-functionalized WSCPs precursors, both of them are usually studied and discussed as comparison for each other. In the following part, we would discuss these two kinds of WSCPs together and present their development and application in organic electronic devices.

The neutral precursor polymer **P5**, **P6** and their quaternized derivatives **P7**, **P8** were used as the emitting layer in PLEDs with the configuration: ITO/poly (3,4-ethylene-ioxythiophene): poly(styrene sulfonic acid) (PEDOT:PSS) or poly(*N*-vinyl carbazole) (PVK)/Polymer/Al (or Ba/Al). Similar to previously reported PLEDs based on the other WSCPs, the devices based on these polymers also exhibited very poor performance. All of these polymers met the same challenge as those traditional polyfluorene homopolymers that the EL emission is very different from their photoluminescence (PL) emission and a new red-shifted emission peak appeared at 500–550 nm due to strong excimer formation[40,41] which has been proved to be one of the main reasons for the poor device performance of polyfluorene-based light-emitting polymers. All of these polymers exhibited similar poor device performance with EQEs less than 0.5%. However, one interesting phenomena was discovered here that all of these polymers showed higher EQEs in the devices with high work function metal Al as a cathode than those with low-work function metals Ba cathode. For example, **P5** showed a maximum EQE of 0.38% in the device with configuration ITO/PVK/**P5**/Al, while a significantly decreased maximum EQE (0.12%) was observed in the device with Ba cathode (device configuration: ITO/PVK/**P5**/Ba/Al). It is well known that low work function metals, such as Ca, Ba *etc.*, are commonly used as the cathode in most of PLEDs to ensure efficient electron injection from cathodes to CPs EML materials, because most of CPs are p-type semiconductors and the PLEDs based on them are usually limited by the low electron affinity and low mobility of electrons.[42,43] Thus, the interesting PLEDs device results of **P5–P8** indicate that these polymers are different from most of the traditional CPs and may dramatically improve the electron injection from high work-function metal cathodes.

P5 was used as ETL in PLEDs with configuration, ITO/PEDOT:PSS/EML/**P5**/Al, where three commercially available RGB light-emitting CPs MEH-PPV, P-PPV and poly (9,9-diolkylfluorene) (PFO) were used as EML and a thin layer of **P5** (3–20 nm) was used as ETL on top of them.[37,44,45] For comparison, two kinds of reference devices ITO/PEDOT:PSS/EML/Ba/Al and ITO/PEDOT:PSS/EML/Al were also made. Since **P5** can be processed from methanol under the presence of small amount of acetic acid and these EML polymers are insoluble in methanol, the mixing between the interfaces of the different polymer active layers can be avoided. Interestingly, the devices results indicated that **P5** showed excellent electron injection properties for all of the RGB polymers. As shown in Table 1, all the three light-emitting polymers exhibited very poor performance in the devices with bare Al as cathode. However, when a thin layer of **P5** was used as electron injection/transfer layer, the device performance was greatly improved. The luminous efficiency (LE) of MEH-PPV device was significantly improved from 0.02 cd A^{-1} with a luminance of 6 cd m^{-2} at a current density of 34.7 mA cm^{-2} to 1.2 cd A^{-1} with a luminance of 454 cd m^{-2} at a current density of 36.7 mA cm^{-2} by using **P5** as ETL. For P-PPV device, using **P5** as electron transfer layer, the device' LE reaches 23.8 cd A^{-1}, with a luminance of 7923 cd m^{-2} at a current density of 33.3 mA cm^{-2}, and it is even better than P-PPV's device with barium cathode, which shows a LE of 20.6 cd A^{-1} with a luminance of 6955 cd m^{-2} at a current density of 35.0 mA cm^{-2}.[37] Similar significant improvements were also found in blue-emitting PFO devices. Fig. 2 showed the current density–luminance–voltage (*J–L–V*), luminance–voltage (*L–V*), external quantum efficiency–voltage (*QE–V*) and current–voltage (*I–V*) characteristics of MEH-PPV based devices. It was notable that the device with **P5**/Al cathode provides much better injection than the neat Al cathode, showing a steeper exponential current increase after turn-on, and higher current at same voltage than that from the neat Al cathode. Moreover, the devices with **P5**/Al bilayer cathode show similar *I–V* characteristics as those devices based on Ba/Al cathode, with a turn on voltage at around 1.6 V and a similar current increase after turn-on, indicating that the high efficiency of **P5**/Al cathode devices is the result of improved electron injection. Moreover, it is found that the insertion of **P5** layer almost has no influence on the polymers' emission profile. All of the three light-emitting polymers show similar EL spectra both in Ba/Al cathode devices and in **P5**/Al cathode devices (Fig. 3). This indicates that the recombination zone of these devices is located in the bulk of EL polymers and **P5** plays a role of electron injection layer. Similar dramatic electron injection ability was also observed in the quaternized polyelectrolytes (**P7**, **P8**), which also show the same promising performance as their neutral precursors when used as electron injection layer in PLEDs.[44]

Since the widely used low work function cathode metals (such as Ca, Ba *etc.*) are highly reactive, they tend to create detrimental quenching sites at areas near the interface between the EML and the cathode. Moreover, the mobile metal ions formed during the cathode deposition could also affect the long-term stability of the devices.[46] Thus, it is desirable to use high work-function metals (such as Al, Ag, or Au) as cathode because of their better environmental stability and simplicity involved for device fabrication. To improve electron injection from high work-function metals into emitting layer, numerous approaches have been reported. For example, by inserting a thin layer of polar or ionic insulating species, such as lithium fluoride (LiF)[47] and caesium fluoride (CsF)[48] or organic surfactants[49] between Al and the light emitting layer, the electron injection from Al cathode could be significantly improved. However, the amino-/ammonium-functionalized polyfluorene WSCPs are very different from the above methods. **P5** does not exhibit metal cathode dependence and can be applied to other high work-function metals.[50] As shown in Table 1, **P5**′ excellent electron injection ability is not limited in Al (φ = 4.30 eV), but also works for other high work-function metals such as In (φ = 4.12 eV), Ag (φ = 4.26 eV), Sn (φ = 4.42 eV), Cu (φ = 4.65 eV), and Au (φ = 5.20 eV). It is

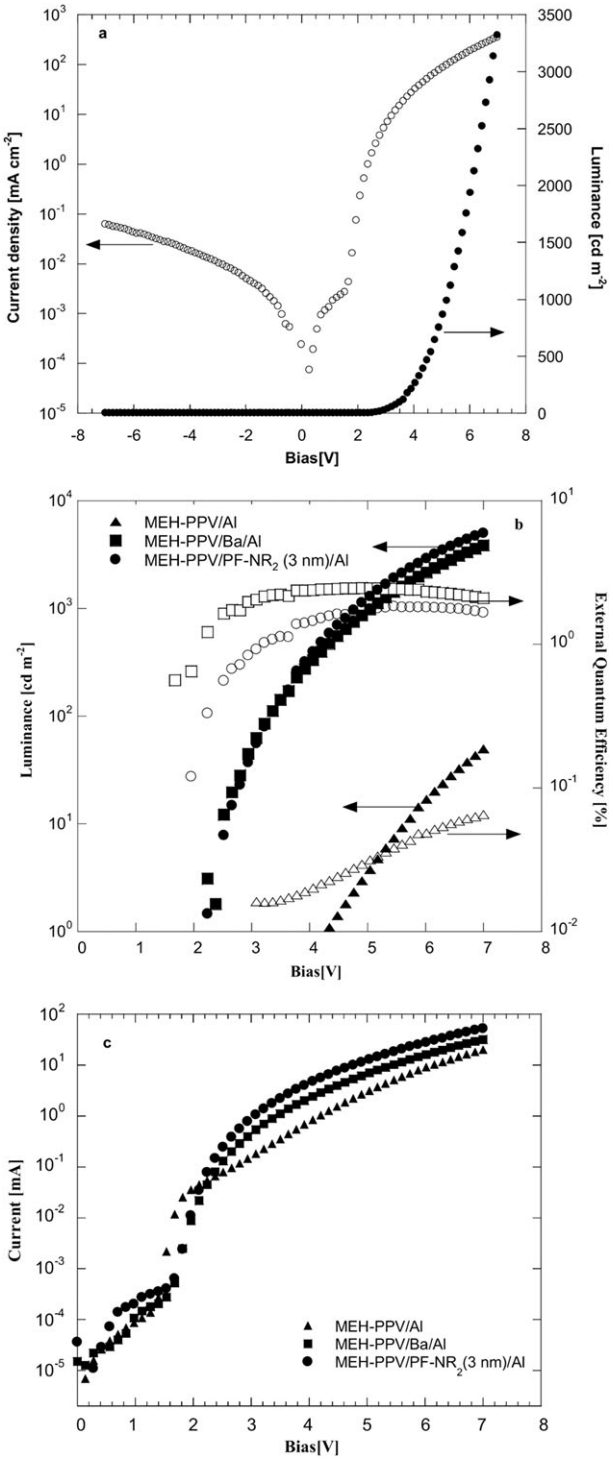

Fig. 2 (a) *J–L–V* characteristic of ITO/PEDOT/MEHPPV/**P5(PF-NR$_2$)**/Al at −7–+7 V bias, (b) *L–V*, *QE–V* (c) *I–V* characteristics of MEH-PPV devices with Al, Ba/Al and **P5**/Al cathodes. Reproduced with permission from ref. 37. Copyright 2004 Wiley-VCH Verlag GmbH & Co. KGaA.

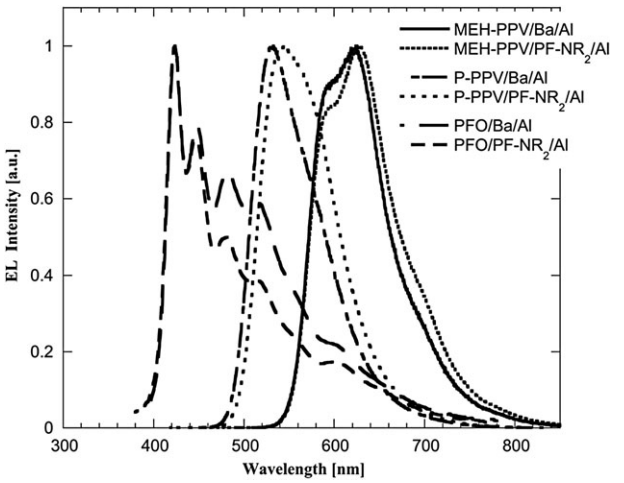

Fig. 3 EL spectra for MEH-PPV, P-PPV and PFO devices with **P5(PF-NR$_2$)**/Al bilayer cathode and Ba/Al cathode. Reproduced with permission from ref. 37. Copyright 2004 Wiley-VCH Verlag GmbH & Co. KGaA.

well known that Au is a most noble metal with a high work-function and has been previously accepted as a good hole injection electrode.[51] Clearly, all of the three RGB polymers MEH-PPV, P-PPV and PFO exhibited very poor device performance in Au cathode devices due to the big difference between their LUMO and the work-function of Au, which indicate a substantial barrier height for electron injection. However, their device performance can be significantly improved by using **P5** inserted between Au and emitting layer as an ETL layer. For example, using **P5** as ETL, P-PPV exhibited an LE of 11.642 cd A^{-1} with a luminance 3648 cd m^{-2} at the current density of 31.3 mA cm^{-2}, which is much better than that of P-PPV in plain Au cathode device, showing a LE of 0.006 cd A^{-1} with a luminance 0.78 cd m^{-2} at the current density of 35.9 mA cm^{-2}. Since gold has an excellent chemical, environmental stability and thermal conductivity, using Au as cathode might open a door for fabrication and patterning of air-stable flat panel displays.

In order to understand the mechanism of the remarkable electron injection ability of these amino-/ammonium-functionalized polyfluorene WSCPs, photovoltaic measurements were carried out for a series of PLEDs with configuration: ITO/PEDOT/MEH-PPV/**P5**/Au or ITO/PEDOT/PVK/PFO/**P5**/Au, which only differ in **P5** layer thickness range from 0–30 nm, to estimate the built-in potential across the devices.[52] Since the anode and the EL polymer layer are identical in all devices, the built-in potential (V_{bi}) of the devices should scale with the change of barrier height at the cathode side. It was found that for ITO/PEDOT/MEH-PPV/**P5**/Au devices, the V_{bi} shifts from 0.15 V to 0.9 V with an increase in the thickness of the **P5** layer employed from 0, 1 nm, 2 nm, 3 nm, 10 nm, 20 nm, 25 nm and 30 nm. A similar phenomenon was also observed in ITO/PEDOT/PVK/PFO/**P5**/Au device, where the V_{bi} increase from 0.45 V to 1.45 V for device with a 30 nm **P5**/Au cathode. It is notable that the V_{bi} can be significantly tuned by insertion of **P5** layer with different thickness, resulting in greatly improved device performance. In combination with the *J–L–V* characteristics of the PLEDs, the obtained results indicate that the enhanced electron injection and the improved device efficiency are due to the reduction of barrier height in the cathode interface. It has been reported that Schottky rule of vacuum level alignment can be broken by strong metal/polymer (organic) interaction, such as the adsorption of

Table 1 Device performances of RGB PLEDs using **P5**/metals as a cathode in device configuration ITO/PEDOT:PSS (PVK)/EL polymer/**P5**/metals. Reproduced with permission from ref. 37, copyright 2004 Wiley-VCH Verlag GmbH & Co. KGaA, and reproduced with permission from ref. 50, copyright 2005 Elsevier

EL polymers	Cathode	Bias/V	Current density/mA cm^{-2}	Luminance/cd m^{-2}	QE (%)	LE/cd A^{-1}
MEH-PPV	Al (φ = 4.30 eV)	4.6	34.7	6	0.02	0.02
MEH-PPV	**P5** (3 nm)/Al	5.2	36.7	454	1.54	1.2
P-PPV	Al (φ = 4.30 eV)	7.7	34.7	115	0.11	0.3
P-PPV	**P5** (20 nm)/Al	8.8	33.3	7923	7.85	23.8
PFO	Al (φ = 4.30 eV)	14.4	34.7	2	0.02	0.01
PFO	**P5** (20 nm)/Al	9.7	30	380	1.62	1.3
MEH-PPV	In (φ = 4.12 eV)	4.8	33	1.1	0.003	0.003
MEH-PPV	**P5** (20 nm)/In	5.9	37.5	98	0.305	0.261
P-PPV	In (φ = 4.12 eV)	4	31	22.4	0.024	0.072
P-PPV	**P5** (25 nm)/In	7.4	29.7	3945.5	4.369	13.299
PFO	In (φ = 4.12 eV)	9	31.2	46.1	0.106	0.148
PFO	**P5** (25 nm)/In	9	29.8	326.2	1.391	1.095
MEH-PPV	Ag (φ = 4.26 eV)	5.1	32.9	0.8	0.003	0.002
MEH-PPV	**P5** (20 nm)/Ag	6.4	35.7	61	0.199	0.171
P-PPV	Ag (φ = 4.26 eV)	4.3	28.7	5.8	0.007	0.02
P-PPV	**P5** (20 nm)/Ag	5.6	29.1	908.5	1.025	3.125
PFO	Ag (φ = 4.26 eV)	20.2	30.3	11.4	0.048	0.038
PFO	**P5** (20 nm)/Ag	15	39.1	122.4	0.398	0.313
MEH-PPV	Sn (φ = 4.42 eV)	6.7	35.7	2.4	0.008	0.007
MEH-PPV	**P5** (20 nm)/Sn	7.6	31.4	66.4	0.246	0.211
P-PPV	Sn (φ = 4.42 eV)	3.9	31	5.8	0.006	0.019
P-PPV	**P5** (20 nm)/Sn	5.8	40.3	1192.8	0.974	2.962
PFO	Sn (φ = 4.42 eV)	20.7	30.1	9.3	0.039	0.031
PFO	**P5** (20 nm)/Sn	16.2	34.1	147.1	0.548	0.432
MEH-PPV	Cu (φ = 4.65 eV)	5.6	33.2	2.5	0.009	0.007
MEH-PPV	**P5** (25 nm)/Cu	8.9	36.4	334.4	1.071	0.918
P-PPV	Cu (φ = 4.65 eV)	3.2	37.1	4.9	0.004	0.013
P-PPV	**P5** (3 nm)/Cu	3.6	35.9	160.4	0.147	0.447
PFO	Cu (φ = 4.65 eV)	16	32.7	14.1	0.089	0.043
PFO	**P5** (25 nm)/Cu	13.5	35.1	416.6	1.509	1.188
MEH-PPV	Au (φ = 5.20 eV)	6.6	166.7	0.8	0.0004	0.0005
MEH-PPV	**P5** (30 nm)/Au	11.8	39.9	377.5	1.240	0.945
P-PPV	Au (φ = 5.20 eV)	13.2	35.9	0.78	0.002	0.006
P-PPV	**P5** (20 nm)/Au	9.4	31.3	3648.0	3.843	11.642
PFO	Au (φ = 5.20 eV)	24.4	32.0	0.6	0.002	0.002
PFO	**P5** (20 nm)/Au	11.8	35.3	495.7	1.778	1.403

molecules on metal surfaces, dipole formation, charge transfer and interface state.[53,54] Thereby, it was proposed that dipole formation is most likely the origin of the reduction of barrier height between Au and EL polymers due to the presence of **P5** layer. As a result, an abrupt shift of vacuum level at the interface was observed and the work-function or surface potential of the metal is altered.

More conceptually straightforward technique such as electroabsorption (EA) measurement was applied to determine the built-in potential in the device.[50] Being a nonlinear optical measurement, the technique is based on the fact that the absorption coefficient of a thin semiconducting layer can be perturbed or modulated by electric field.[55–57] Besides, EA can be used to identify various excitonic energy levels and measure the locations of various charged states in the band gap,[58,59] such as traps, dopants, bipolarons and polarons. This technique is of particularly interest for organic optoelectronic devices based on thin films, where application of small bias across the film can produce electric field of order of 10^7 V m^{-1}. Such electric field can significantly modulate the absorption coefficient, and take great advantage over other indirect approaches in quantifying the internal electric field in a device structure. Its high reliability lies in direct measurement and noninvasion to the device and had been demonstrated be valid for probe the built-in field in polymer/metal structure.[60–62] To be exact, EA signal of a sample, representing the relative change of the optical transmission under the application of electric field, is proportional to the imaginary part of the optical third-order susceptibility Im $\chi^{(3)}(\hbar\omega)$ and the square of the electric field, then the EA response due to an applied ac bias, $E = E_{DC} + E_{AC}\cos\omega t$, follows,

$$\frac{\Delta T}{T}(\hbar\omega) \propto \mathrm{Im}\chi^{(3)}(\hbar\omega)\{E_{AC}^2[1+\cos(2\omega t)]/2 + 2E_{AC}E_{DC}\cos(\omega t) + E_{DC}^2\}$$

Thus, in presence of built-in field, the EA response at the fundamental harmonic frequency is both modulated by V_{AC} and the actual DC component ($V_{DC} - V_{bi}$) across the device. Consequently, changing the DC component and finding the voltage at which the EA response at fundamental frequency vanishes can determine the built-in field. With a thin **P5** layer inserted between EML polymer and Al, the built-in potential deduced from the EA response as a function of DC bias exceeding 2000 mV was observed,[50] in comparison to a V_{bi} of 1200 mV for plain Al device. This result is fully consistent with that of the previous photovoltaic measurement.[37] For a MEH-PPV/**P5**/Al device, a built-in potential about 2300 mV

corresponds to a considerable increase over that of the neat Al cathode (1200 mV, which is approximately equal to the difference between the work functions of ITO/PEDOT and Al in a flat-band configuration. Significant enhancement of the built-in potential indicates that the effective barrier height for the electron injection is substantially lowered by the insertion of a **P5** layer between Al and the emitting layer, thereby leading to a more balanced injection of electrons and holes.

Besides **P5–P8**, which have a large band gap and exhibit blue-emitting both in solution and in solid states, amino-/ammonium-functionalized polyfluorene copolymers (**P9–P18**) were also developed (Scheme 3).[63–67] Several different narrow band gap (NBG) heterocyclic monomers, such as 2,1,3-benzothiadiazole (BTDZ), 4,7-di-2-thienyl-2,1,3-benzothiadiazole (DBT), 2,1,3-benzoselenadiazole (BSeD), 4,7-di-2-thienyl-2,1,3-benzoselenadiazole (DBSe), were incorporated into the polyfluorenes' main chains to tune the optoelectronic properties of resultant polymers. By this strategy, the emission of the polymers can be readily controlled by choosing different type of NBG monomers and tuning the ratio of added NBG monomers, which can be well controlled during the polymerization. Efficient energy transfer was observed among these polymers and the polymers' solid state emissions were dominated by the NBG units even when their contents are as low as 0.5%. The polymers' PL emission were tuned from blue for **P5** and **P7** to green for **P9** and **P13** by using BTDZ NBG units (544–580 nm), and to red for **P10** and **P14** by using DBT NBG units (625–682 nm). The polymers based on selenium-containing NBG units (BSeD, DBSe) exhibit more red-shifted emissions compared to their analogues based on sulfur-containing monomers (BTDZ, DBT). **P11** and **P15** show green to yellow emissions with emission peak at 579–597 nm, while **P12** and **P16**'s emission peak were red-shifted to around 750 nm in near IR region. Clearly, without significant changing the polymers' structure, the polymers emission can be tuned from blue to near IR and covered the entire visible region. Moreover, the polymers' PL efficiency in the film was also significantly improved. For example, with 0.5% BTDZ units copolymerized on the main chain, **P9**'s PL efficiency increased to 74.6%, which is much higher than that of **P5** (37.3%). It was also found that the polyelectrolytes always show a red-shifted UV-vis absorbance spectra and (PL) emission spectra relative to their neutral precursor in thin solid films, which is probably caused by their aggregation properties. Consequently, the PL efficiencies of the polyelectrolytes are much lower than their neutral precursors, due to the severely quenching effect of their counterions. PLEDs based on **P9–P18** also show much improved device performances compared to the devices based on **P5–P8**, which is consistent with their significantly enhanced PL efficiency. And it was found that all these polymers exhibited similar dramatic electron injection ability as **P5–P8** and showed excellent device performances in devices with high work-function metal Al cathodes. Among these polymers, **P9** shows the highest external QE of 3.24% with a luminance of 494 cd m^{-2} at current density of 13 mA cm^{-2} in the device configuration: ITO/PVK/**P9**/Al,[63] whereas the maximum QE of **P5** is only 0.38% with a luminance of 22 cd m^{-2} in the same device structure.[36] Several factors contribute to the improved device performance. Firstly, the excimer formation among these polymers was greatly suppressed by the added NBG units. Hence, these added NBG units also acted as a "trap" among the polymer main chain and can significantly suppress interchain excimer formation in the devices. It should be pointed out that these polymers showed good device performances even with Au as cathode.[67,68] **P13** (with 0.5% BTDZ) exhibit an EQE of 0.73% with a luminance of 497 cd m^{-2} at the current density of 58 mA cm^{-2} in device with configuration: ITO/PVK/**P13**/Au, which is similar to those of devices with Al, Ba/Al cathode.[68] By incorporating small amount of hole transporting triphenylamine units into the polymer main chains, **P17** and **P18** show improved device performance in Au cathode devices with EQEs more than 1%.[67] it is expected that the improved electron injection from high work-function metals for these polymers were also came from the amino-/ammonium-groups on their side chains *via* dipole formation at the metal/polymer interface.[37,50] As a result, **P9–P18** can also be applied as the ETL to improve the electron injection from high work-function metal cathodes in PLEDs. For example, **P10** which is red emitting as EML can be used as ETL to greatly improve device performance of green-emitting polymer P-PPV with Al cathode (ITO/PEDOT:PSS/P-PPV/**P10**/Al) without affecting the EL emission of P-PPV.[64] **P15** was used in a highly efficient multilayer PLED based on a red-emitting iridium complex ($Ir(DMFPQ)_2$) with configuration: ITO/PEDOT:PSS/PVK/PFO:2-(4-biphenylyl)-5-phenyl-1,3,4-oxadiazole (PBD):$Ir(DMFPQ)_2$/**P15**/cathode, where the PBD was used as dopant to improve the electron transporting of the EML and Al or Ba/Al were used as the cathode.[69] Photovoltaic studies showed that the open circuit voltage (V_{oc}) of devices were increased by the insertion of **P15** indicating that the electron injection from Ba/Al was also improved (Device configuration: ITO/PEDOT:PSS/PVK/PFO:PBD:$Ir(DMFPQ)_2$/**P15**/Ba/Al), resulting in a promising device performance with an EQE of 18% and LE of 9.8 Cd/A and an emission peak of 636 nm at a current density of 1.1 mA cm^{-2}.[69] Considering the unique solubility in environment-friendly solvents and the encouraging devices performance of these polymers, these amino-/ammonium-functionalized polyfluorene copolymers are promising candidates for next generation of light emitting copolymers in PLED flat panel display applications.

In order to take the advantage of phosphorescent metal complexes which can fully utilize both singlet and triplet excitons in LEDs,[70] amino-/ammonium-functionalized polyfluorene copolymers based on phosphorescent metal complexes (**P19–P24**) were also developed (Scheme 4).[71–75] However, it was found that the energy transfer among them was not as efficient as that of corresponding fluorescent NBG units based polymers **P9–P18** and the PL efficiencies of these polymers are also very low. Moreover, there is almost not any phosphorescent metal complex units' emission observed among the ammonium functionalized polymers **P20** and **P22**, and both of them exhibited very low PL efficiencies (less than 2%). Hence, most of these polymers exhibited poor device performances in PLEDs. One exception is **P24**,[75] where the doped phosphorescent metal complex units were attached to the side chains other than in the main chains. **P24** showed an improved energy transfer ratio as well as higher PL efficiencies (20%–40%) compared to the others (**P19–P23**). A relative

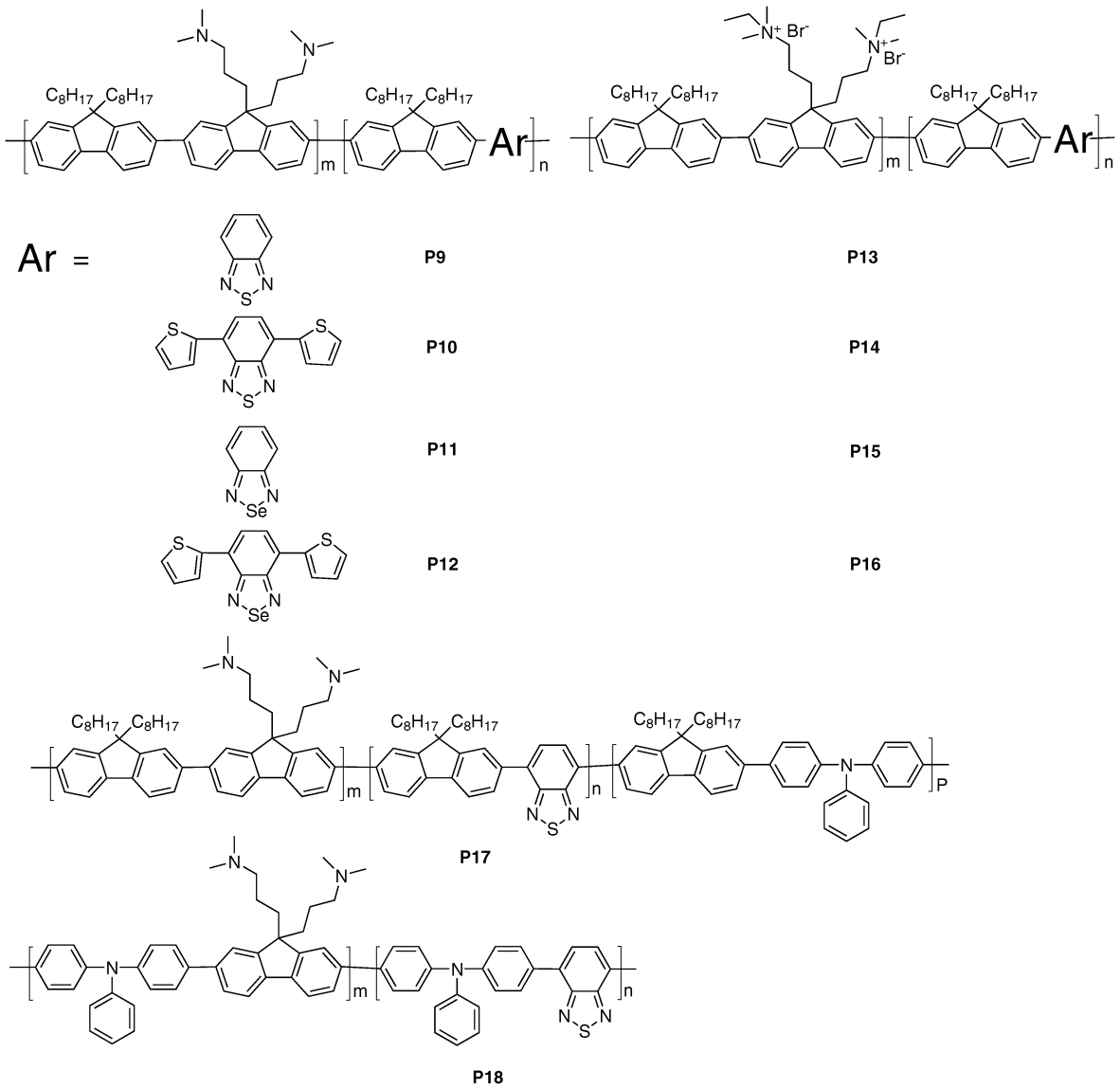

Scheme 3 Molecular structures of **P9–P18**.

high device performance with an EQE of 5.50% was obtained by **P24** based PLED with configuration: ITO/PEDOT:PSS/PVK/**P24**/Ba/Al.[75] Despite of their relative poor device performance when used as EML, all of these polymers show good electron injection abilities in devices, due to the amino/ammonium-groups on their side chains. For example, **P19** was used as high efficiency ETL layer in P-PPV based PLEDs with Au cathode, where the devices' EQE were significantly improved from 0.0033% to 1.67%.[71] And **P23** also can greatly improve P-PPV based PLEDs' performances when used as ETL.[74] It is interesting to note that the added small amount (<15%) of fluorescent NBG units or phosphorescent metal complexes do not affect the electron injection ability of these polymers.

Ma *et al.*[76] reported the use of a copolymer of oxadiazole and ammonium-functionalized fluorene (**P25**) as ETL in PLEDs (Scheme 5). **P25**, with oxadiazole, shows a LUMO level of −3.19 eV and a HOMO level of −6.38 eV, which are very different from polyfluorene homopolymers, indicating that it is a good electron transport material for PLEDs. The electron injection transport properties of **P25** were examined in PLEDs with device structure ITO/PEDOT/EML/**P25**/Ba/Al, where PFO, PFO-BT and MEH-PPV were used as the EML materials. For comparison, the devices without ETL were also fabricated. It was shown that the device performances were significantly improved by using polymer **P25** as ETL layer with decreased turn on voltages, improved efficiencies and dramatically increased luminance, which is resulted from the improved electron injection and hole-blocking capability of **P25**. Moreover, the addition of **P25** layer may move the recombination zone away from the cathode and thereby eliminates cathode quenching. And the atomic force microscope (AFM) studies showed that the **P25** film exhibited a much rougher surface than those of EML polymers, which may also contributed to the enhanced electron injection, because the contact area between ETL and metal cathode was increased.

Oh *et al.*[77–79] reported a series of ammonium functionalized WSCPs **P26–P29** as ETLs in PLEDs. Different from the other

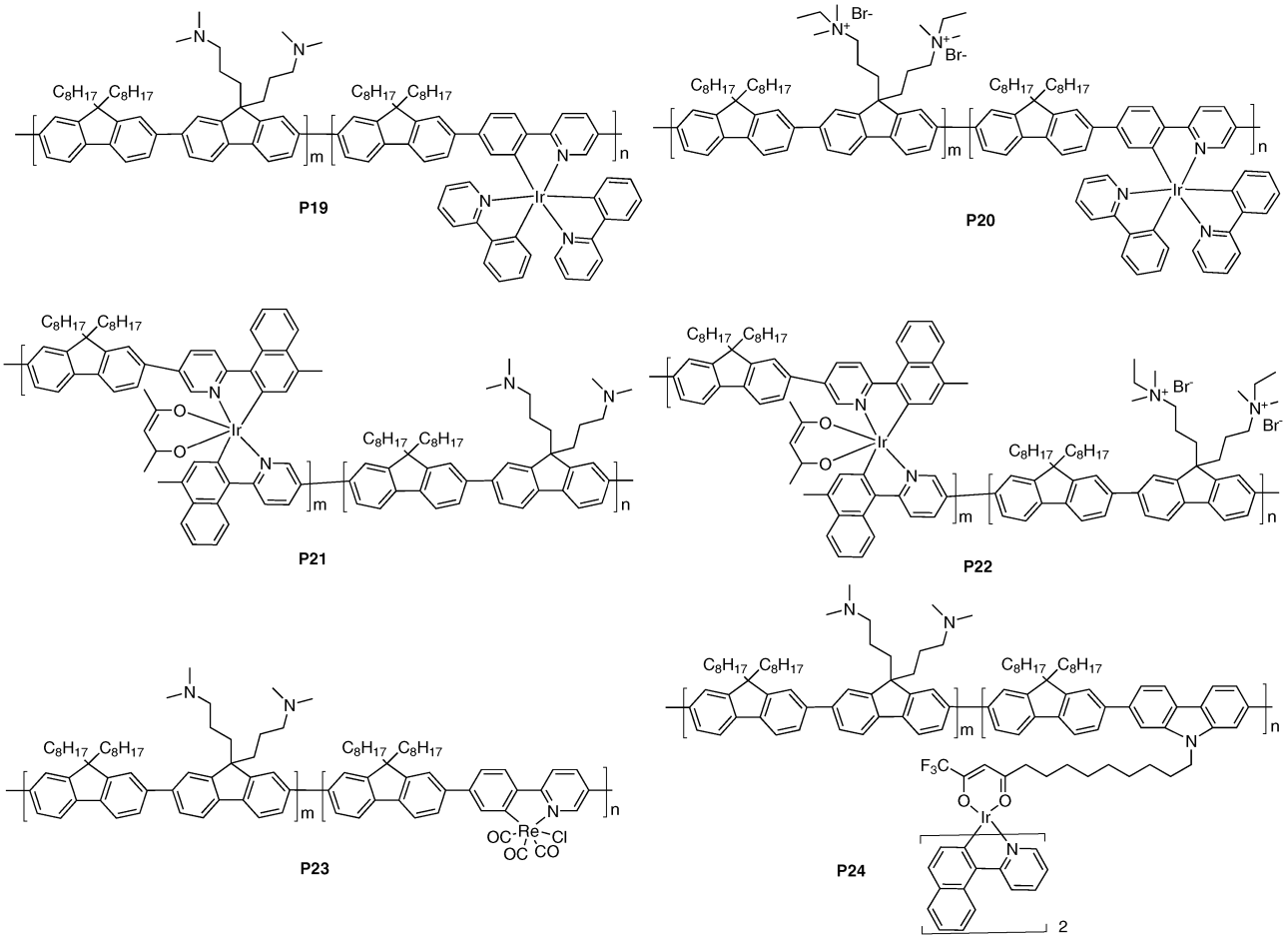

Scheme 4 Molecular structures of **P19–P24**.

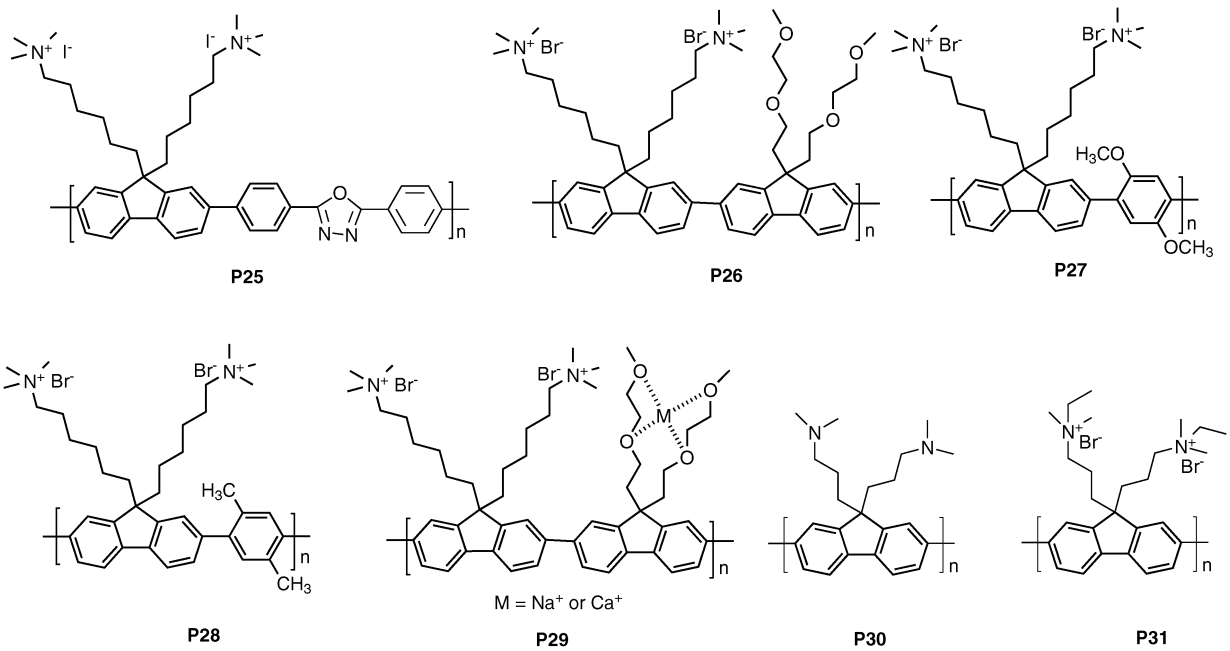

Scheme 5 Molecular structures of **P25–P31**.

ammonium functionalized WSCPs discussed above, **P26–P28** were obtained from the reaction of neutral precursor polymers with bromine atom terminated side chains and trimethylamine. By using different co-monomer, **P26–P28** exhibited

different optical and electrochemical properties. **P26–P28** were used as ETL in MEH-PPV based PLEDs with configuration: ITO/PEDOT:PSS/MEH-PPV/ETL/Ag.[77] By using **P26–P28** as ETL, the device performance was greatly improved and photovoltaic studies also showed that the open circuit voltage (V_{oc}) of devices were significantly increased by the insertion of these polymers, indicating that the electron injection barrier height was dramatically lowered. It was noted that **P26** exhibited much better electron injection abilities than the other two polymers **P27** and **P28**. For the device using **P26** as ETL, the turn on voltage was reduced from 6.5 V to 3.1 V and EQE was increased from 0.005% to 0.2%, which is one order of magnitude higher that those of devices using **P27** and **P28** as ETL. It was proposed that the ethylene oxide side groups of **P26** exhibit similar functionality as poly(ethylene oxide) (PEO) in light-emitting electrochemical cells (LECs), which can transport mobile ions in the devices.[80] Indeed, a much slower response on the increase of luminance under certain bias was observed in **P26** based devices compared with all the other devices (Fig. 4), implying bromide ions migration through the ethylene oxide groups in **P26**. As a result, mobile bromide ions could migrate more easily in **P26** and led to a large space charge field, which can reduce the charge injection barrier.[81] Later on, it was found by the same group that **P26**'s electron injection ability can be further improved by binding Na^+ or Ca^{2+} ions on its ethylene oxide side chains (**P29**).[79] Binding between Na^+ or Ca^{2+} ions and the ethylene oxide units were confirmed by the binding energy of Na^+ or Ca^{2+} with oxygen atoms using X-ray photoelectron spectroscopy (XPS). When **P29** was used as ETL in PLEDs based on a green-light-emitting polyfluorene derivative with configuration: ITO/AlPF11/Dow Green/ETL/Al, much better device performance was obtained with LE of 11.0 cd A^{-1} for **P29**-Na^+ and 15.4 cd A^{-1} for **P29**-Ca^{2+}, respectively. In comparison, the LE of device with **P28** ETL or bare Al cathode were only 3.0 cd A^{-1} and 0.02 cd A^{-1}, respectively. Photovoltaic measurements showed that the devices with **P29** ETL exhibited higher open circuit voltages (1.20 V for **P29**-Na^+ ETL device and 1.64 V for **P29**-Ca^{2+} ETL device) than those of **P28** ETL device (0.53 V) and bare Al cathode device (0.24 V), which is attributed to the enhanced dipole formation or space charge field and the consequent lower barriers. The LEC behavior was also observed among **P29** ETL devices, where a gradual increase in the luminance of the devices under certain bias was observed compared to the device without ETL.

Wang *et al.*[82] reported the synthesis of amino-functionalized polyfluorene homopolymer **P30** and its quaternized derivative **P31**. Compared to **P5–P8**, **P30** and **P31** have a high ratio of amino- or ammonium-groups on their side chains. As a result, **P31** shows much better solubility up to 100 mg mL^{-1} and a high PL efficiency of 44% in water. The electron injection ability of **P31** was examined in a small molecule based OLED with configuration: ITO/NPB/Alq_3/**P31**/Al. it was found that the device's LE reaches 1.6/cd A^{-1}, which is three times greater than the reference device with Al cathode, indicating the good electron injection ability of **P31**.

2.2 Ammonium-functionalized WSCPs with different counterions

It has been shown that the optoelectronic properties of WSCPs (conjugated polyelectrolytes) are greatly influenced by the counterions on their side chains.[19,28–30] Thus, it is possible to tune WSCPs' optoelectronic properties for various applications by controlling the counterions without changing their main chain structure. Using a series of typical cationic WSCPs, poly[(9,9-bis-(6′-*N*,*N*,*N*-trimethylammonium)hexyl)-fluorene-*alt*-4,7-(2,1,3-benzothiadiazole)] (**P32**-X, where X is the charge compensating anions, Scheme 6), Yang *et al.*[83] studied effect of the counterions X on the optoelectronic properties of **P32**. Quantum yield of photoluminescence of the obtained WSCPs in solid film and in water roughly scale with the size of counterion (3–5% for **P32**-Br *versus* 22–41% for **P32**-$BArF_4$), while in solvent such as DMSO, a quantum yield of 35–45% was observed for all of the WSCPs. The authors attributed the higher quantum yield in solid state of **P32** with larger counterions to the increased average interchain distance which may result in decreased levels of PL self-quenching. As revealed by dynamic light scattering experiments in water solution with a concentration in range of 6.3×10^{-6} M to 1.2×10^{-5} M, the effective diameter for **P32**-Br and **P32**-$BArF_4$ are 353 nm and 73 nm, respectively, which reverse to the mass of the repeat unit of Br^- (742 g mol^{-1}) and $BArF_4^-$ (2308 g mol^{-1}). The much smaller particle size of **P32**-$BArF_4$ indicated the existence of a much reduced aggregation of **P32**-$BArF_4$ in water, which can be attributed to a reducing driving force for packing as a result of hydrophobic contacts with water. The influence of charge compensation ions on the hole mobility was investigated by conductive atomic force microscopy. It was found that hole mobility for **P32**-Br, **P32**-$BArF_4$ and the corresponding precursor material poly-[9,9-bis(6-bromohexyl)fluorene-*alt*-4,7-(2,1,3-benzothiadiazole)] are 3.4×10^{-4}, 1.1×10^{-5} and 6.5×10^{-6} cm^2 V^{-1} sec^{-1}, respectively, suggesting that the charge compensation ions on the side chain did not cause negative impact on their charge transport along the backbone.

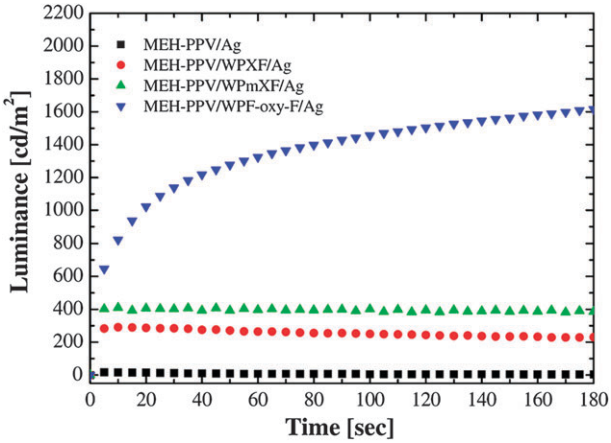

Fig. 4 Luminance as a function of time of each device with ETL (WPF-oxy-F:**P26**, WPmXF:**P27** or WPXF:**P28**) biased at 5 V, except MEH-PPV/Ag biased at 10 V. Reproduced with permission from ref. 77, Copyright 2007 Elsevier.

The performance of WSCPs as the ETL in PLEDs can be strongly influenced by the charge compensating ions.[84] As shown in Fig. 5, for a series of PLEDs with device structure of ITO/PEDOT:PSS/MEH-PPV/**P33**-X (X = Br, CF_3SO_3, BIm_4 and $BArF_4$)/Al, superior device performance was obtained

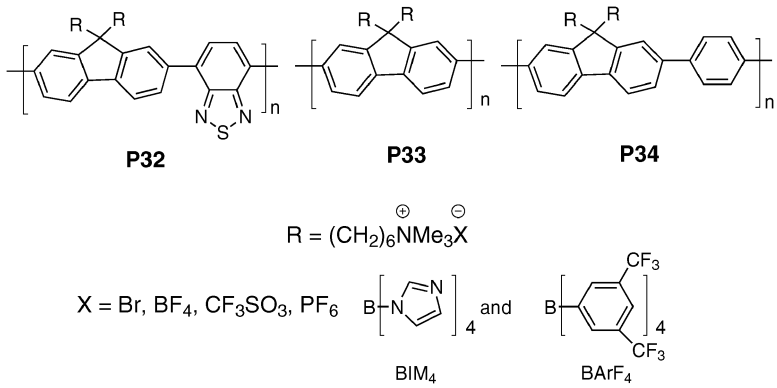

Scheme 6 Molecular structures of **P32–P34**.

when the counterions were BIm_4^-, while the device with **P33**-$BArF_4$ as ETL only showed a LE of order of 10^{-3} cd A^{-1}, which was even much less efficient than the control device. Correlating with the device performance, the built-in potential across the device as determined by photovoltaic measurement were 1.65 V for **P33**-CF_3SO_3/Al, 1.60 V for **Ba**/Al, 1.55 V for **P33**-BIm_4^-/Al, 1.45 V for **P33**-Br/Al, 1.15 V for Al device and 0 V for **P33**-$BArF_4$/Al device, respectively.

Hoven *et al.*[85] found that the response time of an ITO/PEDOT:PSS/EML/**P34**-BIm4/Al device, which is defined as the time taken by a devices to reach the 50% of its steady current density (or luminance) at a given voltage, is strongly dependent on the applied voltage. The response time was determined as 0.5 s, 2.5 s, 6.1 s, and 20 s for 6 V, 5 V, 4.5 V and 4 V, respectively (Fig. 6), which was several orders of magnitudes longer than that of typical PLEDs[86,87] and the PLEDs with WSCPs as ETL reported previously.[36,37] The authors attributed the slow response time to the formation of a hybrid device upon the incorporation **P34**-BIm4, in which mixed ionic and electronic conduction are involved, and characterized with features both from PLEDs and LECs.[88] Besides strong dependence on the applied voltage, the response time of the ITO/PEDOT:PSS/PFO/**P34-BIm4**/Al device was found to be correlated with the thickness of ETL. As can be seen in Fig. 7, steeper response was attained as the thickness of the ETL decreased. For example, at an applied bias of 4.5 V, the response time decreased with the ETL thickness: 10.4 s for 30 nm, 9.2 s for 25 nm, 8.2 s for 15 nm and 6.1 s for 10 nm. This observation can be attributed to the ion motion in the WSCPs upon application of electric field. The authors atributed the operation mechanism of the devices is similar with the operation of LECs.[88] However, it was pointed out by deMello *et al.*[89] that ionic charge redistribution occurs throughout the bulk of the polymer film might make device response time substantially retarded and changing with counter-ion size. Thereby, slow response time might be due to charge redistribution in the ETL layer and it does not require the presence of an electrochemical oxidation/reduction process or doping in LECs. Furthermore, both of the LEC mechanism and the ionic charge redistribution picture require an external bias to achieve an overall steady-state but nonequilibrium charge neutrality, which is in contrast with our early observation that the interfacial dipole moment is induced by the strong interaction between the high work function metal and the polar group of the polyelectrolytes.[50] It is important to note that, as shown in Fig. 2a, light emitting was observed only when the ITO was positively biased, indicating the ITO/PEDOT:PSS/Emissive layer/**P5** (**P6**, **P7**, **P8**) (20 nm)/Al devices operate as a diodes rather than a LEC.

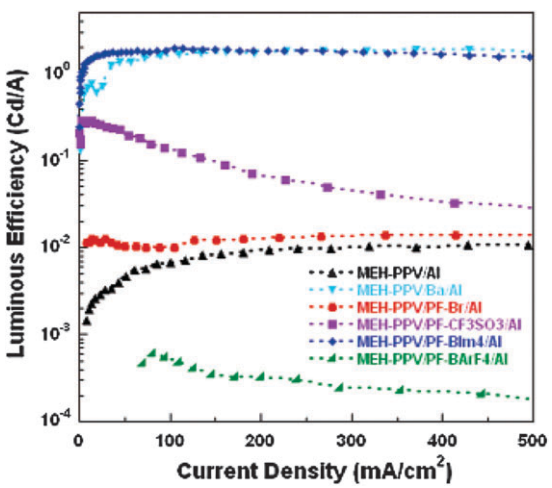

Fig. 5 Luminous efficiency *vs.* current density characteristics for different cathodes: **P33**-$BArF_4$/Al (green), Al (black), **P33**-Br/Al (red), **P33**-CF_3SO_3/Al (purple), Ba (light blue), and **P33**-BIm_4/Al (blue). Reproduced with permission from ref. 84. Copyright 2006 American Chemical Society.

On the basis of previous work, Hoven *et al.*[90] further proposed a model for the electron injection from bilayer cathode consisting of WSCPs and high work function metal, in which ion motion plays a major role. The model involves the combination of hole accumulation at the active layer/ETL interface due to the hole blocking properties of ETL and the subsequent ionic redistribution across the ETL due to displacement of anions in the ETL. As a result, the electric field across the emissive layer and the ETL were screened, thus the electron injection barrier height was dramatically reduced, leading to an efficient electron injection from high work function metals. According to the model, the internal electric field is screened and nearly zero in both layers, thus the electron current are diffusion dominated rather than drift dominated, together with ion motion across the ETL thin

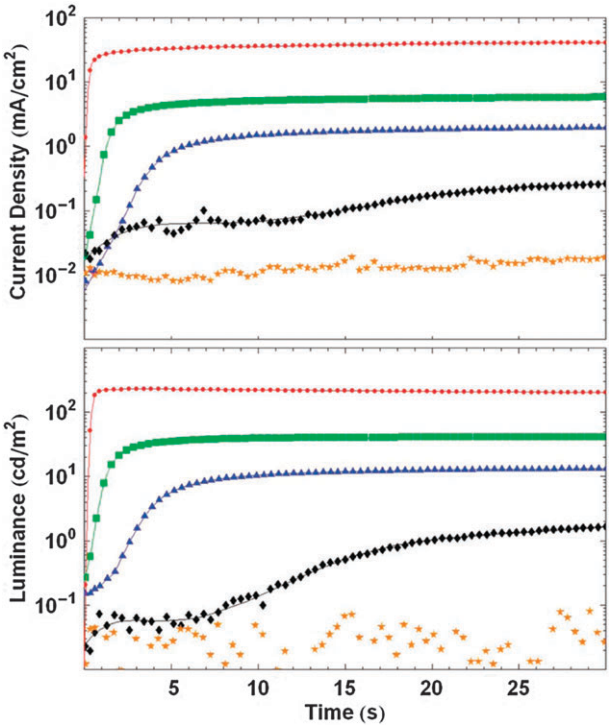

Fig. 6 The transient response of current density and luminance for a ITO/PEDOT/PFO/**P34**-BIm4/Al LED with constant applied bias: 6 V (red circles), 5 V (green squares), 4.5 V (blue triangles), 4 V (black diamonds). Shown in orange stars are the data from a device without the **P34**-BIm4 layer at 5 V. Reproduced with permission from ref. 85. Copyright 2007 American Chemical Society.

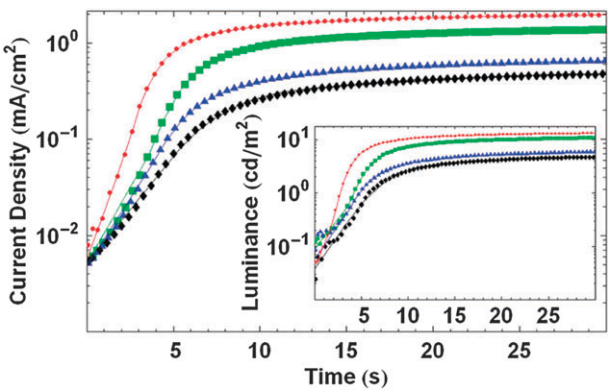

Fig. 7 Transient response of J and L (inset) for an ITO/PEDOT/PFO/**P34**-BIm4/Al PLEDs with 4.5 V applied with different **P34**-BIm4 thicknesses: 10 nm (red circles), 15 nm (green squares), 25 nm (blue triangles), 30 nm (black diamonds). Reproduced with permission from ref. 85. Copyright 2007 American Chemical Society.

layer, leading to a slow response of the device. Transient response of current density and luminance as a function of the PLEDs architecture supported the redistribution of ions within the ETL, that the ETL acted as a hole blocking layer and the recombination happened at the interface. In addition, very recently, direct probe of the electric field in the ITO/PEDOT/PFO/**P34**-BIm$_4$/Al device using electroabsorption spectroscopy was reported,[91] revealing that the electric field in the EML layer was screened by the hole accumulation.

2.3 Diethanolamino-functionalized WSCPs

A series diethanolamino-functionalized WSCPs **P35–P38** were also developed as ETL for high efficiency PLEDs (Scheme 7).[92–95] The motivation for this work is to combine the advantages of neutral surfactants (such as PEO, PEG *etc.*) and conjugated polymers as ETL in PLEDs. It has been reported that the PEG-like neutral surfactants can dramatically improve the devices' performances when used as ETL in PLEDs, due to the enhanced electron injection from Al cathode and the suppressing of the emission quenching by cathode metal.[96,97] It was also found recently by Guo *et al.*[98] that deposition of an Al electrode causes the oxidation at the surface of EML, which can be prevented by inserting a PEG-based neutral surfactant buffer layer. Moreover, the X-ray photoelectron spectroscopy results indicate that the formation of a carbide-like (negative carbon) thin layer is critical to the injection of electrons through the Al cathode. As a result, PEG-based neutral surfactants show promising properties as cathode interfacial modification layer in OLEDs. Compare to previously reported conjugated polyelectrolytes ETL, these neutral surfactants can avoid the influence of counter ions and are more favorable for PLEDs with long life time. However, there is also obvious drawback for using PEG type ETL materials that the thicknesses of PEG layer in devices must be carefully controlled due to their insulate nature, which may cause the complexity of the device fabrication. Moreover, PEG-based neutral surfactants only works for Al metal cathode and could not be applied to other high work-function metals. To overcome this problem, diethanolamino-functionalized WSCPs **P35–P38** were designed. Different from previously reported none-conjugated neutral surfactants, all of these polymers comprise a conjugated main chain and a surfactant-like side chain. As a result, all these polymers keep the excellent electron injection ability of those neutral surfactants, while the conjugated main chain endow them a good conductivity which is an obvious advantage over those insulate PEG-based neutral surfactants. Moreover, the amino groups on the side chains also significantly improve the electron injection from Al and other high work-function metal Ag or Au.[50] Owing to all these advantages, all of these materials show promising properties when used as ETL in PLEDs.[92–95] For example, **P35** was used as high efficiency ETL in PLEDs with configuration: ITO/PEDOT:PSS/PF3B:PHF (1 : 5)/cathode, where a green-emitting polymer blends was used as EML and **P35**/Al, Al or Ca/Ag were used as the cathodes.[92] Fig. 8 showed the devices' *J–L–V* characteristics and luminous efficiency *vs.* current density characteristics. Clearly, the device with **P35** as EIL shows a significantly better electron injection property than the device uses only Al cathode, with a steeper exponential current increase after turn-on, and higher current density at the same voltage. The device with **P35** ETL showed a lower turn on voltage ($\sim$3.6 V) and much higher brightness at the same voltage (L = 21 800 cd m^{-2} at 6 V) than those obtained from the device with neat Al as cathode (turn on voltage at $\sim$5.4 V, L = 52 cd m^{-2} at 6 V). Moreover, the device with **P35** ETL showed an even better performance than the one using low work-function metal Ca as cathode. The maximum brightness of **P35**/Al device reaches 34 900 cd m^{-2},

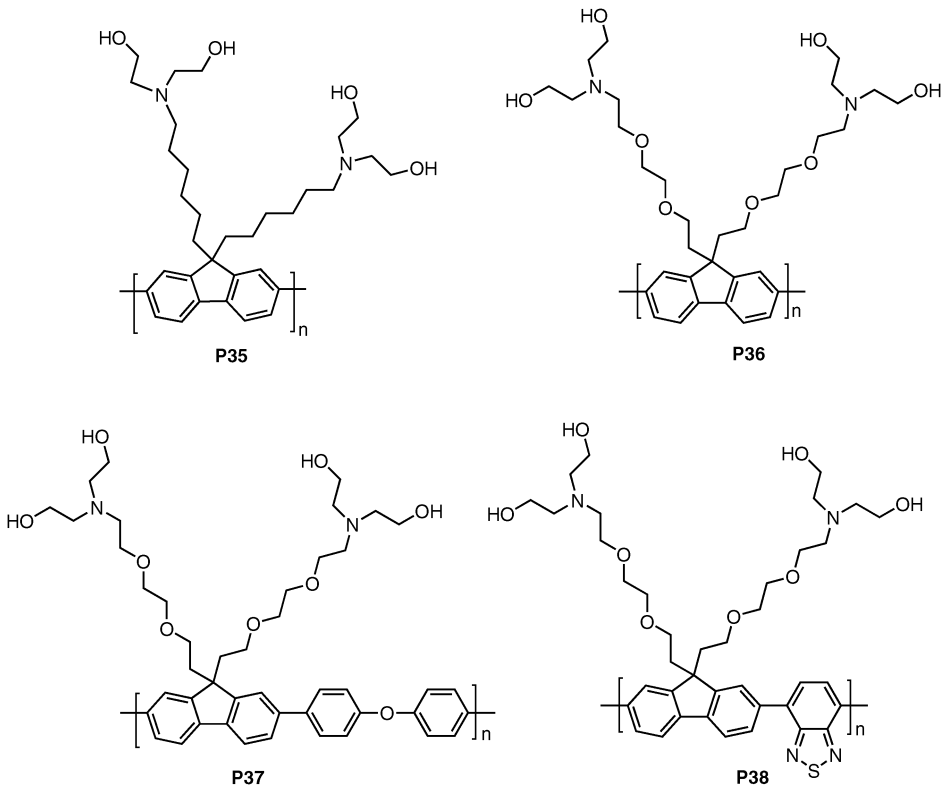

Scheme 7 Molecular structures of **P35–P38**.

which is much higher than that obtained from the device using Ca/Ag as cathode (<4000 cd m^{-2}), which is probably due to the prevention of cathode quenching. Fig. 8b showed that the **P35**/Al device exhibited the highest LE, which is almost two orders of magnitude higher than that of Al cathode device and one order of magnitude higher than that of Ca/Ag cathode devices.

The dramatic electron injection ability of **P35** originated from its surfactant-like side chains. Both the hydroxyl groups[96,97] and amino groups[37,50] of its side chains can interact with Al cathode to reduce the barrier height for electron injection at the interfaces and lead to better electron injection. Indeed, the photovoltaic measurements results showed that the V_{oc} moves from approximately 0.2 V for a plain Al device to around 1.6 V for the device with an additional **P35** layer, indicating that the effective barrier height for electron injection is substantially lowered by inserting a **P35** layer between Al cathode and emission layer. This leads to more balanced population of electrons and holes for more efficient recombination. Moreover, due to the amino groups of its side chains, **P35** also works very well for the other high-work function metals such as Ag or Au. For example, the device with **P35**/Au cathode (ITO/PEDOT:PSS/PF3B:PHF [1 : 5]/**P35**/Au) showed a LE of 2.74 cd A^{-1} at a current density of 35 mA cm^{-2}, whereas there was hardly any light could be detected from the device with neat Au as cathode. When WSCPs were used as ETL in phosphorescent PLEDs, it was found that the device performance are highly depend on the processing condition of WSCPs ETL, because the commonly used electron transporting dopants, such as 2-(4-biphenyl)-5-(4-*tert*-butylphenyl-1,3,4-oxadiazole) (PBD) and 1,3-bis[2-(4-*tert*-butylphenyl)-1,3,4-oxadiazol-5-yl]-benzene (OXD-7), can be seriously washed out by the alcohol. Consequently, the phosphorescent PLEDs with ETL

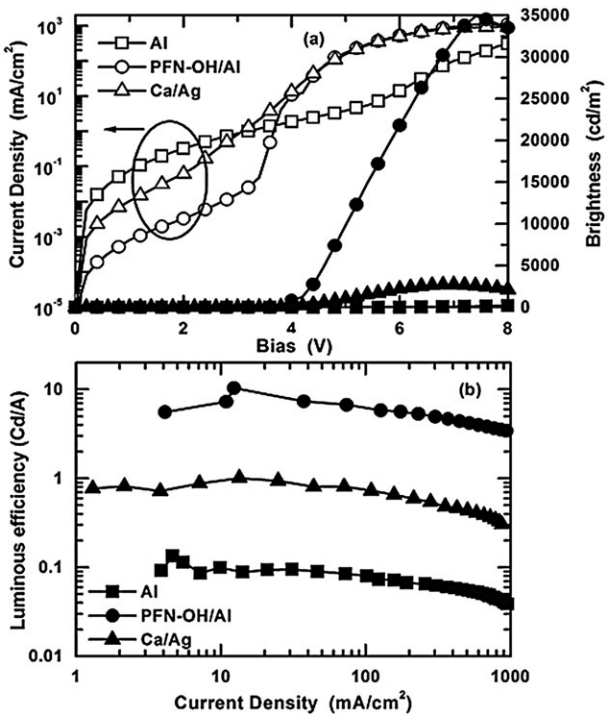

Fig. 8 (a) *J–L–V* characteristics and (b) Luminous efficiency *vs.* current density characteristics of the devices with Al, PFN-OH(**P35**)/Al and Ca/Ag cathodes. (Device configuration ITO/PEDOT:PSS/PF3B:PHF [1 : 5]/cathode). Reproduced with permission from ref. 92. Copyright 2007 Wiley-VCH Verlag GmbH & Co. KGaA.

processed from alcohol exhibited very poor device performance. However, the erosion of small molecular dopants can be greatly suppressed by adding small amount of water into the alcohol.[92,93] As a result, the devices' performances were dramatically improved by using ETL processed from alcohol/water co-solvents. For example, when **P35** (processed from ethanol–water 4 : 1 solvent) was used in the device with the structure of ITO/PEDOT:PSS/PVK:PBD (30%):*tris*(2-phenylpyridine)iridium $Ir(ppy)_3$(1%)/**P35**/Al, the device exhibited a high LE of 43.0 cd A^{-1} at a current density of 0.6 mA cm^{-2} with a brightness of 257 cd m^{-2}.[92] The device with **P35**/Al cathode showed even much better performance than that of reference device with CsF/Al cathode (LE = 23.1 cd A^{-1}), which has been proved to be ideal cathode for phosphorescent PLEDs compared to those low work-function metals (such as Ca).[99]

P36–P38 have the same surfactant-like side chain but with different main chains, which are good candidates for exploring the main chain effect on the electron injection properties of these WSCPs ETL materials.[93] **P36** has a fully conjugated main chain as typical polyfluorene homopolymers, while **P37**'s conjugation length is effectively confined by the oxygen atoms on the main chain leading to a larger band gap than **P36**.[100] Different from **P36** and **P37**, **P38** has a fully conjugated but electron-deficient main chain as poly(9,9′-di-n-octylfluorene-alt-benzothiadizole) (PFBT) which is a typical electron transporting material with good electron mobility.[101,102] Optical and electrochemical studies showed that the HOMO energy level of **P36**, **P37** and **P38** is −5.7 eV, −5.9 eV, and −5.9 eV, respectively, while their LUMO levels were −2.8 eV, −2.6 eV and −3.5 eV for **P36**, **P37** and **P38** respectively. According to the energy levels of these three polymers, **P38** should have the best electron-injecting ability compared to **P36** and **P37**. Moreover, as material for electron injection, the hole-blocking ability of **P37** and **P38** should be better than **P36**, due to their relatively high HOMO level. However, when used as ETL in a red-emitting polymer PFDBT02[103] based PLEDs with the configuration of ITO/PEDOT:PSS/PVK/PFDBT02/ETL/Al, it was found that both **P36** and **P37** work very well as efficient ETL in PLEDs and the devices with **P36** and **P37** ETL exhibited even much better performance than the device with Ba/Al cathode. However, **P38** did not show an obvious ETL effect in device and the PLED with **P37**/Al cathode exhibited performance as poor as the device with neat Al cathode (Fig. 9).[93] Similar results were also observed among the phosphorescent devices, where the devices with **P36** and **P37** exhibited excellent performances and **P38** did not work as an ETL. Photovoltaic studies showed that both **P36**/Al and **P37**/Al cathode device exhibited a larger V_{oc} of 2.1 V and 2.2 V, respectively, than those of the Al (1.1 V) and Ba/Al (1.8 V) cathode devices, while the **P38**/Al cathode device showed a much smaller V_{oc} (1.3 V), indicating no reduction of the electron injection barrier from Al cathode by inserting **P38** layer. Since all the polymers have a same side chain, these results indicate that the main chain also plays an important role on the electron injection ability of these WSCPs ETL materials.

Moreover, the unique solubility of these polymers also offers the possibility to enhance electron injection and conduction by doping it with water-soluble alkali or alkaline earth

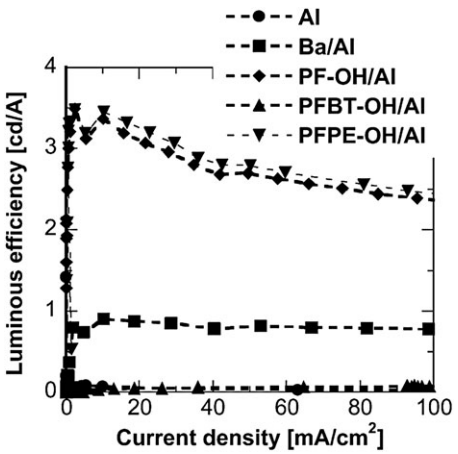

Fig. 9 Luminous efficiency *vs.* current density characteristics of the devices with different cathodes. (Device configuration: ITO/PEDOT:PSS/PVK/PFDBT02/cathode) (PF-OH:**P35**, PFPE-OH:**P36**, PFBT-OH:**P37**). Reproduced with permission from ref. 93. Copyright 2009 Wiley-VCH Verlag GmbH & Co. KGaA.

metal salts, which have been used as n-type dopants in OLEDs.[104,105] Compared to the conjugated polyelectrolytes, these neutral polymers are ideal hosts for *n*-doping by metal salts because they do not involve the complexity of the counter ions in conjugated polyelectrolytes. It was found that the electron injection ability of these polymers was indeed significantly improved by doping them with water soluble alkali or alkaline earth metal salts.[95] For example, both undoped and LiF/Li_2CO_3 (5%) doped **P37** were used as ETLs in the typical blue-emitting phosphorescent complex bis[(4,6-di-fluorophenyl)-pyridinato-N, C^2] (picolinate) Ir(III) (FIrpic) based blue-emitting PLEDs with the configuration of ITO/PEDOT:PSS/FIrpic(7%):PVK:OXD-7(30%)/ETL)/Al). The turn on voltage of the device with **P37** ETL was decreased from 8.2 V to 6.8 V or 6.4 V upon doping with 5% LiF or Li_2CO_3, respectively. At the same time, the devices' performances were also significantly improved with greatly increased EQEs and LEs upon doping. The studies on the electron-dominate device (ITO/Al/PVK:OXD-7 (30%)/ET/Ba/Al) and the hole-dominated device (ITO/PEDOT/PVK:OXD-7 (30%)/ETL/Au) indicate that electron current density of the devices with LiF or Li_2CO_3 doped ETL are much higher than that of the device with undoped ETL, which means that the electron transporting ability of **P37** ETL is significantly enhanced upon doping. Moreover, the results of the hole-dominated device clearly showed that the hole-current density of the **P37** ETL significantly decreased upon doping. Therefore, it is clearly indicated that LiF or Li_2CO_3 doped **P37** ETL possesses enhanced electron injection/transporting ability compared to that of undoped **P37** ETL, resulting in much improved device performance. This strategy can be potentially applied to further improve the performance of WSCPs ETL materials.

2.4 Other WSCPs as ETL in PLEDs

Anionic WSCPs **P39** (Scheme 8) was also developed[106] and applied as ETL in PLEDs.[107,108] **P39-Na** was used as efficient ETL in devices with configuration: ITO/PEDOT:PSS/MEH-PPV/ETL/Al, which was compared to the other two

WSCPs ETL materials **P32-Br** and **P34-Br**. The reference devices with Al or Ba/Al cathode were also made for comparison. By using **P39-Na** as ETL, the device's turn on voltage was decreased from 4.5 V for the device with neat Al cathode to ~2.5 V, and the LE of the device was also greatly improved to the level of the device with low work-function metal Ba/Al cathode, indicating that **P39-Na** is very effective at modifying the barrier for electron injection from Al cathode. Meanwhile, the device with **P34-Br** ETL also showed an improved device performance compared to the Al cathode device, but still much poorer than that of device with **P39-Na** ETL. Similar to the WSCP with the same main chain **P38**,[93] the device with **P32-Br** ETL exhibited the LE as low as the device with neat Al cathode, indicating **P32-Br** is not an effective ETL for Al cathode. The mobilities of these polymers were measured in electron-only devices with configuration of Al/**P39-Na**, **P32-Br** or **P34-Br**/Ba/Al, using the space-charge limited current (SCLC) model. Despite the same main chain, the electron mobility of **P39-Na** (1.5×10^{-7} cm^2 V^{-1} s) is two order's lower than that of **P34-Br** (1.2×10^{-5} cm^2 V^{-1} s). Moreover, with the same side chain, **P32-Br**'s electron mobility (1.1×10^{-6} cm^2 V^{-1} s) is one order's lower than that of **P34-Br**. That was attributed to the nonplanar disposition of the benzothiadiazole and fluorene repeat units.[102] Most interestingly, despite of the lowest electron mobility, **P39-Na** exhibited the best electron injection property in the device, which is possible due to that the electron injection is more efficient in the ITO/PEDOT:PSS/MEH-PPV/**P39-Na**/Al device. Later on, the **P39** with different counterions were developed through the ion exchange way and used as ETL in PLEDs.[108] When they were used as EML in the devices with configuration: ITO/PEDOT:PSS/**P39**/Al, obvious LEC characteristics were observed where the devices emitted light under both forward and reverse bias conditions and the turn on voltage of the devices are very close to the band gap of **P39**. All of these polymers with different counterions were used as ETL in device with configuration: ITO/PEDOT:PSS/Supper-yellow/ETL/Al to investigate the counterions effect on their electron injection properties. It was found that the **P39** with alkali metal counterions (Li^+ and Na^+) show better device performances with lower turn-on voltages, higher maximum luminance, and higher luminous efficiencies at fixed current densities as compared to the devices without ETL or with **P39**-H or **P39**-NH_4 ETL. It was proposed that metallic cation polyelectrolytes exhibited stronger LEC effect compared to the nonmetallic cation polyelectrolytes, thereby leading to a more effective electron injection effect for metallic cation polyelectrolytes. Among all of them, **P39-Na** showed the most effective electron injection ability and the LE of the device with **P39-Na** ETL reached 2.40 cd A^{-1}. This was decreased to 1.27 cd A^{-1} when the Na^+ concentration of **P39** was decreased to 50% (50% deprotonation), indicating that the concentration of Na^+ ions in the ETL layer directly influence the device performance. All these results indicate that the electron injection ability of WSCPs are influenced by many factors, including their main chain structures, side chain pendant groups, the type of charge and their counterions.

Zhou *et al.*[109,110] reported the developing of a phosphonate group functionalized WSCPs **P40** and its use as efficient ETL

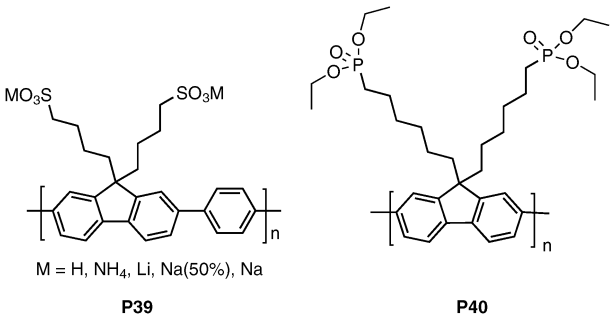

Scheme 8 Molecular structures of **P39–P40**.

materials in PLEDs. The polar phosphonate groups of **P40** endow it both a good solubility in alcohol and excellent electron injection ability from Al cathode. The electroluminescent property of **P40** was examined in the device with configuration: ITO/PVK/**P40**/cathode, where Al, Ca, Mg or Ag was used as cathode. Among them, the Al cathode device exhibited the best performance with the highest maximum LE of 4.0 cd A^{-1} and lowest turn on voltage of 4.6 V, indicating the electron injection from Al cathode was greatly enhanced by **P40**. The electron-only device Al/**P40**/cathode (Al, Ca, Mg or Ag) also showed that the highest electron current density was achieved in the Al cathode device. It was proposed that phosphonate groups have a strong coordinating power to metal cathodes that result in the formation of an ultrathin interfacial layer, which can facilitate efficient electron injection from the cathodes. Hence, it was shown that using **P40** as ETL can greatly improve the PFO based PLEDs' performance, which is even better than that of device with Ca/Al cathode. Most interestingly, the device with **P40**/Al cathode exhibited a much better stability against moisture and oxygen than Ca/Al cathode device.[110] It indicates that the PLEDs' life time may be significantly improved by using WSCPs as ETL, while maintaining the excellent device performances.

3. Unique applications in organic electronic devices

3.1 Applications in high-efficiency white-emitting PLEDs

White-emitting polymer light-emitting diodes (WPLEDs) have attracted considerable attentions due to their potentially applications in full-color flat panel displays, back-lighting sources for liquid-crystal displays, and solid-state lighting.[111,112] The distinctive advantages of WSCPs in fabrication multilayer PLEDs were also applied to high-efficiency WPLEDs. Gong *et al.*[113] reported the application of water–ethanol-soluble sulfonated PVK (PVK-SO_3Li) as the HTL and water–ethanol-soluble sulfonated PBD (*t*-Bu-PBD-SO_3Na) as the ETL in a high efficiency multilayer WPLEDs with configuration: ITO/PEDOT:PSS/PVK-SO_3Li/EML/*t*-Bu-PBD-SO_3Na/Ba/Al, where a blend of polyfluorene derivatives and Iridium complexes were used as the EML. It was found that charge injection/transport and charge recombination of the devices was significant enhanced by using the WSCPs HTLs and water–ethanol soluble ETL. The resulted WPLEDs emitted pure white light with Commission Internationale de l'Eclairage (CIE) coordinates closed to (0.33, 0.33) and exhibited a high

LE of 10.4 cd A^{-1}. Compared to the WSCPs HTL materials, the WSCPs ETL materials are more widely used in fabrication of high efficiency WPLEDs.[114–119] However, as discussed above, the devices' performance are highly depend on the processing condition of ETLs, due to the erosion of the small molecular dopants.[93,114,115] An *et al.*[114] reported high efficiency WPLEDs based on **P5** ETL with the configuration: ITO/PEDOT:PSS/PVK:OXD-7:FIrpic:Irpiq/**P5**/Al, where the sky-blue-emitting complex FIrpic and red-emitting complex iridium bis(1-phenylisoquinoline) (acetylacetonate) (Ir(piq))-are co-doped into PVK host as EML and small molecular electron transport material OXD-7 is also doped into EML to improve electron transport of the EML. The solvents for processing **P5** varied from water–methanol 6V/1V to 0V/1V and it was found that the device with **P5** processed from water–methanol 1V/3V as ETL exhibited the best device performance with a maximum LE of 18.5 cd A^{-1}, a maximum luminance of 8672 cd m^{-2} and a pure white emission with CIE (0.321, 0.345), while the device with **P5** processed from methanol exhibited the poorest performance with a maximum LE of 1.0 cd A^{-1} and a maximum luminance of 351 cd m^{-2}. The photovoltaic measurements results indicated that the devices with ETL processed from different solvents showed similar open circuit voltages, indicating electron injection barrier height of these devices are similar. Hence, the electron injection abilities of **P5** ETLs processed from different solvents are similar. The UV-vis absorbance studies indicated that the OXD-7 dopants in the EML can be severely washed out by methanol solvent, while this can be greatly suppressed by using water–methanol with proper ratio as co-solvents for processing ETL. Similar phenomenon was also reported by Xu *et al.*[115] that using an oligomer model compound of **P33-BIm4** as ETL in WPLEDs with the similar device structure: ITO/PEDOT:PSS/PVK:OXD-7:FIrpic:Irpiq/ETL/Al. Also, the device with ETL processed from water–methanol 1 V/3 V co-solvent exhibited the best performance with a LE of 15.1 cd A^{-1} and a maximum luminance of 11890 cd m^{-2}.

Zhang *et al.*[116] reported high-efficiency WPLEDs by using yellow-emitting osmium complex (Os–Y) doped into a blue fluorescent polymer as the emissive layer and **P35** as the electron injection layer sandwiched between the emissive layer and Al cathode. The device with the configuration of ITO/PEDOT:PSS/PVK/EML/**P35**/Al exhibited efficient white emission at the CIE coordinates of (0.33, 0.34) and a maximum LE of 16.9 cd A^{-1} and maximum brightness of 22 100 cd m^{-2}. By using different EML materials, WPLEDs with better performances were fabricated based on **P35** ETL.[117] Sky-blue phosphorescent iridium complex FIrpic and orange phosphorescent osmium complex (Os-R) are co-doped into PVK host as the EML to achieve white light emission in the device of ITO/PEDOT:PSS/EML/**P35**/Al. Similar to the other WSCPs ETL materials, it was found that the device with **P35** processed from water–ethanol (1/4 v/v) solution exhibited a much better performance that the device with **P35** processed from ethanol solution. The maximum luminance efficiency of the devices with different cathodes follow the trend Al (0.62 cd A^{-1}) < **P35** (ethanol)/Al (4.83 cd A^{-1}) < Ba/Al (6.18 cd A^{-1}) < **P35** (water–ethanol)/Al (20.7 cd A^{-1}).[117] Moreover, the WPLEDs' performance based on **P35** can be further improved by inserting active metal Ba between the **P35** and Al cathode. The turn-on voltages were decreased from 4.5 V for **P35**/Al cathode devices to 3.9 V for device with **P35**/Ba/Al cathode, indicating the electron injection from cathode was further enhanced. Thus, the highest power efficiency of **P35**/Ba/Al cathode device was improved to 14.5 lm/W at a brightness of 171 cd m^{-2}, which is comparable to the power efficiency of the incandescent light bulbs.

The performance of WPLEDs based on WSCPs ETLs can be further greatly improved by using the salts doping strategy.[118] Li_2CO_3 doped **P36** was used as ETLs in WPLEDs with configuration: ITO/PEDOT:PSS/PVK:FIrpic:Os–O:OXD-7/ETL/Ba/Al, where phosphorescent iridium complex FIrpic and orange phosphorescent osmium complex (Os–O) are co-doped into PVK host as the EML for white light emission. 30% OXD-7 is incorporated to improve electron transport of the EML. Thus, to avoid the erosion of OXD-7 dopants, the co-solvent of water–methanol 1V/4V was used to process all the ETLs. The Li_2CO_3 dopant concentrations in **P36** were tuned from 0% to 30%. Fig. 10 showed the typical *J–L–V* and luminous efficiency-power efficiency-current density (*LE–PE–J*) characteristics of the devices. It was found that the devices with Li_2CO_3 doped ETL showed significantly lowered turn-on voltage and higher current densities under the same driving voltage than that of the un-doped device, indicating that the transporting ability of **P36** ETL is enhanced upon doping with Li_2CO_3. Consequently, the devices with doped ETL exhibited much better performance than the one without doping. However, the device with 30% Li_2CO_3 doped **P36** ETL exhibited much poorer performance and *J–L–V* characteristics, indicating that electrical property of the **P36** ETL is severely interfered under high doping concentration. It is consistent with the morphological changes observed in the AFM study, where 30% Li_2CO_3 doped **P36** film had a much rougher surface than the others and showed the obvious formation of large aggregates. The electron-dominated device (ITO/Al/PVK:OXD-7/ETL/Ba/Al) and the hole-dominated device (ITO/PEDOT/PVK:OXD-7/ETL/Au) results indicated that Li_2CO_3 doped **P36** ETL possesses enhanced electron transport/hole-blocking ability compared to that of the un-doped **P36** ETL, resulting in much improved device performance (Fig. 11). Among all the devices, the device doped with 15% Li_2CO_3 exhibited the best performance with a maximum forward viewing LE of 36.1 cd A^{-1} and PE of 23.4 lm/W which corresponds to a maximum total viewing LE of 61.4 cd A^{-1} and PE of 39.8 lm/W for solid-state lighting application where all photons are taken into account for illumination.[120] Even at a practical surface luminance of 500 cd m^{-2}, the PE of the device is 23.3 lm/W, which is much higher than those obtained from the incandescent lighting sources. Moreover, all devices exhibit stable white light emission under different driving voltages and the corresponding CIE coordinates are around (0.38, 0.38), which is important for illumination application. It is interesting that all of these WPLEDs exhibited comparable performance to those reported from the state-of-the-art vacuum deposited small molecule WOLEDs, which originated from the amazing properties of those WSCPs ETL materials.

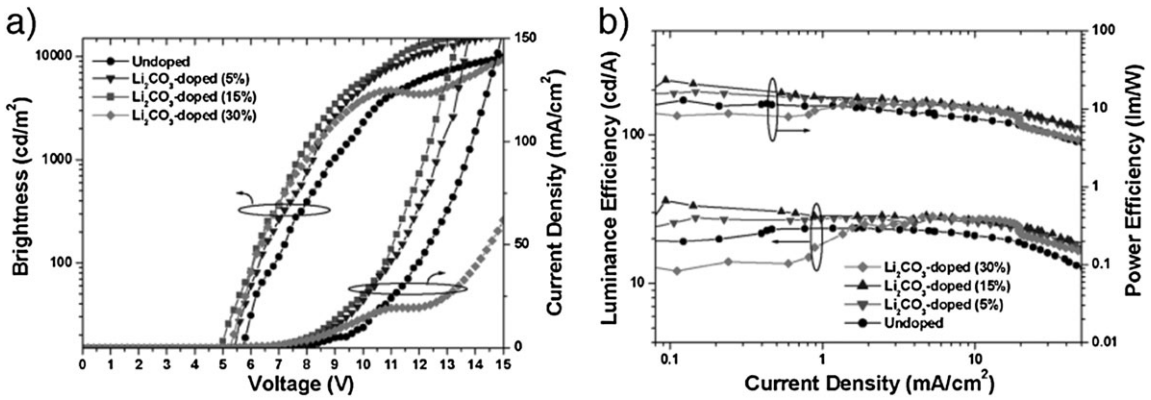

Fig. 10 *J–L–V* characteristics (a) and LE and PE *vs.* current density characteristics (b) of the devices with different ETLs. Reproduced with permission from ref. 118. Copyright 2009 Wiley-VCH Verlag GmbH & Co. KGaA.

3.2 Inverted top-emitting devices

Besides the state-of-the-art PLEDs, the WSCPs also offer many opportunities to realize new device structure, such as the inverted top-emitting organic light-emitting diodes (ITEOLEDs).[121] ITEOLEDs normally have a reflective cathode at the bottom and a transparent anode on the top, which can assure a high aperture ratio in the active matrix OLEDs (AM-OLEDs) and is also highly desirable with n-channel thin-film transistors (TFTs) backplanes in AM-OLEDs, especially for amorphous silicon TFTs that cannot produce adequate p-channel TFTs.[122,123] For PLEDs, there are big challenges to realize this kind of inverted top-emitting devices structure. Firstly, stable high work-function metals need to be used as the bottom cathode to sustain the solution processed top organic layer, which will result in a large electron injection barrier between the organic layer and the metal cathode. Moreover, the underneath ETLs may be destroyed by the solution processed subsequent emitting layer since most of the ETL materials used in PLEDs are soluble in the same solvent as for emitting materials. Both of the challenges can be overcome by the newly developed WSCPs materials which have a unique solubility in high polar solvents and excellent electron injection ability from high work-function metal cathodes. Hou *et al.*[121] reported the fabrication of inverted top-emitting PLEDs by using a bilayer cathode from the alcohol soluble **P13** (with 0.5% BTDZ units) in the device with the configuration ITO/Al/**P13**/MEH-PPV/Au, where a 100 nm thick Al metal layer was deposited by thermal evaporation to serve as the bottom cathode and a 20 nm thick semitransparent Au metal anode was deposited by thermal evaporation to serve as the top anode. Since **P13** has a totally different solubility from MEH-PPV, solution-processing of MEH-PPV layer would not influence the prepared ETL layer. In addition, **P13** can significantly increase the electron injection from Al cathode. As a result, the device with 20 nm **P13** as ETL exhibited excellent performance with an EQE of 2.71% and a LE of 1.6 cd A^{-1} with a luminance of 1640 cd m^{-2} at the current of 102 mA cm^{-2}. This is much better than that of the top emitting device without **P13** ETL, which only showed an EQE of 0.009% and a LE of 0.005% cd A^{-1}.

3.3 All printed PLEDs

It is well known that PLEDs can be processed by spin-coating or ink-jet printing technique *via* solution processing, which is a key advantage compared to small molecular organic semiconductors based OLEDs. However, the metal cathodes of PLEDs still need to be processed *via* vacuum deposition in most cases. Zeng *et al.*[124] reported the use of **P5** as ETL and solution processed Ag paste as the cathode to fabricate high efficiency all printable PLEDs (Fig. 12). Ag paste is a kind of

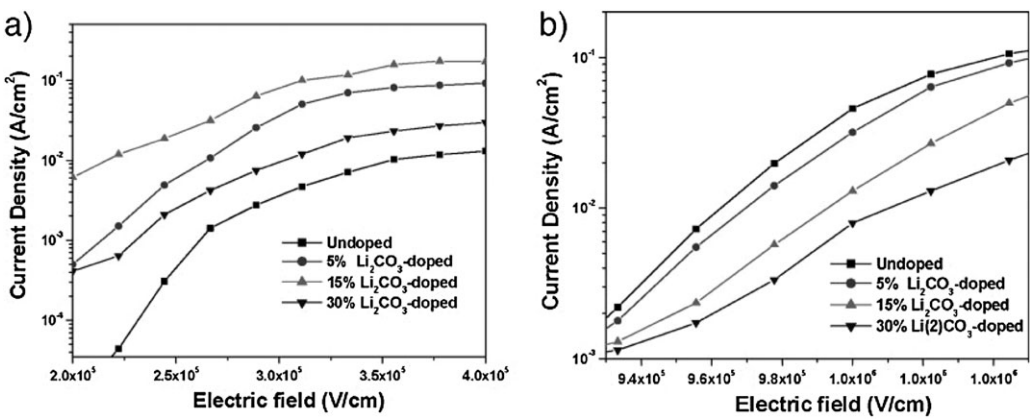

Fig. 11 Current density *versus* electric filed intensity characteristics of the single carrier devices. (a) electron dominated device (b) hole dominated device. Reproduced with permission from ref. 118. Copyright 2009 Wiley-VCH Verlag GmbH & Co. KGaA.

conductive glue and can be deposited from solution as cathode and the electron injection from Ag can be greatly enhanced by **P5**.[50] As a results, the devices with **P5**/Ag paste showed comparable device performances to those devices with Ba/Al, **P5**/Ag (by thermal deposition) cathodes. For example, as shown in Fig. 13, the P-PPV based green-emitting device ITO/PEDOT:PSS/P-PPV/**P5**/Ag paste exhibited a significantly decreased turn on voltage (4.8 V) compared to that of device with Ag cathode (9.4 V), indicating the electron injection from Ag paste cathode is greatly enhanced by **P5** ETL. The Ag paste cathode device's EQE is even better than that of device with Ba/Al cathode (Fig. 13b) and showed a maximum LE of 7.8 cd A^{-1} with a maximum brightness more above 10 000 cd m^{-2} at 12.5 V. Similar excellent device performances based on **P5**/Ag paste cathodes were also observed among PLEDs with blue-emitting polymer PFO or red-emitting polymer PFO-DBT15 EMLs. It is interesting that the WSCPs allow the successful fabrication PLEDs exclusively by printing technique without vacuum deposition involved. All of these results will open a way to achieve all printable roll to roll polymer based organic electronic devices.

3.4 As Interfacial modification layers in PSCs

Solar cells based on a blend of semiconducting polymer and fullerene derivatives have attracted a lot of attention in recent years because they can produce inexpensive electricity directly from the sun due to their ease of fabrication and inherent low cost of solution processing.[3,4] As a result of continuous efforts, the power conversion efficiency (PCE) of polymer solar cells had increased over the last decade and had been shown to exceed 6%,[125,126] obtained through development of new materials or optimization of processing techniques. To further improve the PCE of PSCs, it is important to enhance the V_{oc}, which is typically hundreds of mV in PSCs and still far away from its upper limit ($\sim$1–2 V, as determined by E_g/e, in which E_g the bandgap of the semiconductor, e the element charge).

Recently, Luo *et al.*[127] demonstrated that the V_{oc} of PSCs based on specific system can be enhanced by up to 0.3 V by using a thin layer of WSCPs as interlayer between active layer and metal electrode. Similar with the device structure of PLEDs using WSCPs as ETL, the solar cells have a configuration of ITO/PEDOT:PSS/Active layer/Interlayer/Al, in which thin

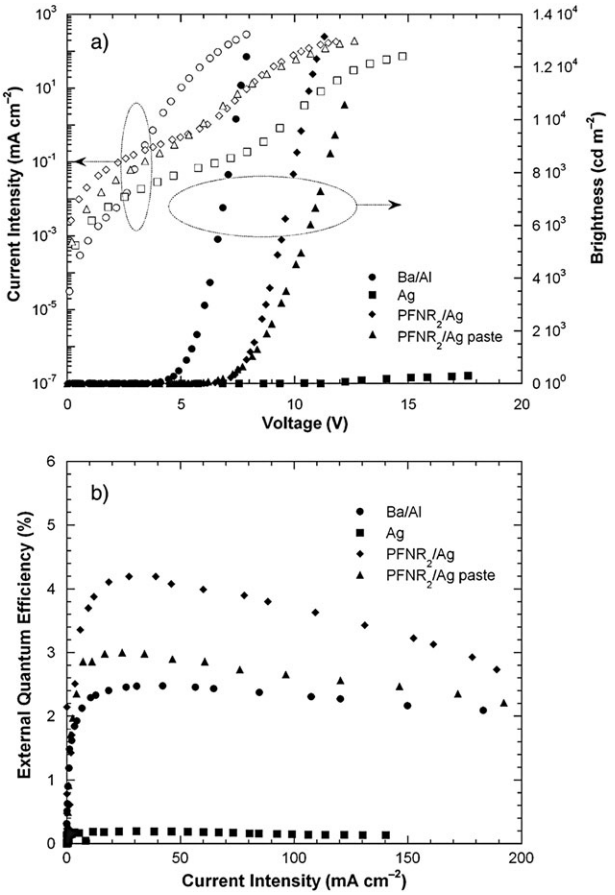

Fig. 13 (a) *J–L–V* and *QE–J* characteristic of P-PPV devices with Ba/Al, Ag, $PFNR_2$ (**P5**)/Ag and $PFNR_2$/Ag-paste cathodes. Reproduced with permission from ref. 124, Copyright 2007 Wiley-VCH Verlag GmbH & Co. KGaA.

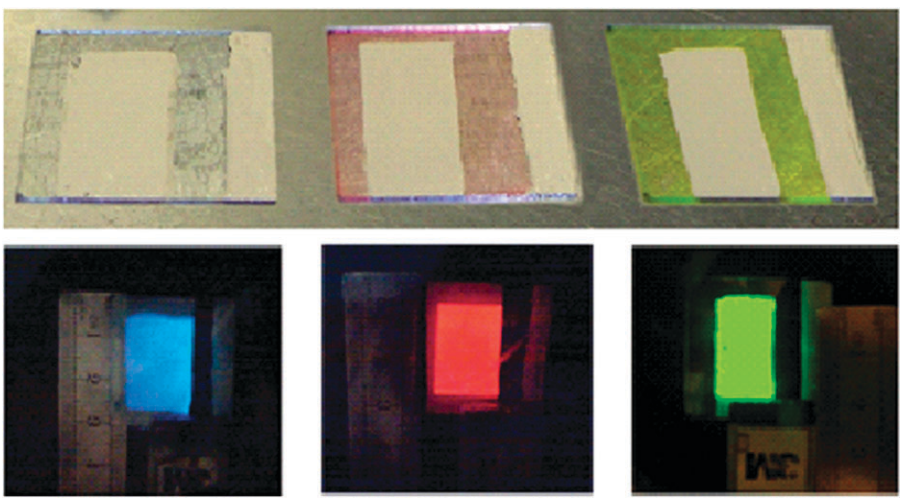

Fig. 12 Photos of RGB PLED devices (3 cm × 3 cm active area) fabricated with a printed Ag-paste cathode. Reproduced with permission from ref. 124. Copyright 2007 Wiley-VCH Verlag GmbH & Co. KGaA.

layer of **P8**[36] and **P14**[64] are incorporated by spin coating. For PSCs based on using poly[2,7-(9,9-dioctylfluorene)-*co*-(4,7-dithien-2-yl)-2,1,3-benzothiadiazole] (PF-DBT35)[128,129] as donor polymer, and [6,6]-phenyl-C_{61}-butyric acid methyl ester (PCBM) as acceptor, it was found that all of the devices with interlayer were characterized with enhanced open-circuit as high as 0.95 ± 0.05 V, while in contrast only a moderate V_{oc} of 0.65 ± 0.05 V was found in the routine cathode devices (Fig. 14). Besides dramatically enhanced V_{oc}, short-circuit current density (J_{SC}) and fill factor (FF) of the devices with interlayer are slightly increased over the control devices, resulting in a double PCE for PFO-DBT35 device. The enhancement of V_{oc} in the devices with interlayer over that of the control devices can be attributed to increased built-in potential across the devices, which is the upper limit of attainable V_{oc} in PSCs.[130] This speculation can be supported by the *J*–*V* characteristics of the devices in the dark (Fig. 14b). Since the diodes turn-on at the voltage at which the internal built-in potential is compensated,[37,50] the fact that a higher turn-on voltage at about 1.0 V was recorded for the devices with interlayer while 0.6 V for the control device (Fig. 14b), indicated an increased built-in potential in the former devices. Furthermore, as shown in Fig. 14b, the electrical leakage for the devices with interlayer is significantly suppressed compared with the control devices, contributed to the increase of V_{oc} too by reducing loss in the V_{oc}.[130]

It is important to note that when PFO-DBT35 was replaced by another donor materials poly[2,7-(9,9-dioctylfluorene)-*alt*-1,1-dimethyl-3,4-diphenyl-2,5-bis (2′-thienyl)silole] (PFO-TST50),[131] similar trend was found, with an enhancement of 0.10–0.15 V in the V_{oc}. However, for the systems using P3HT or MEH-PPV as donors, no enhancement in V_{oc} was found although overall device performance can be slightly improved. The reason responsible for such significant donor polymer dependence in V_{oc} enhancement is not clear so far, which probably can be attributed to a substrate-dependent accumulation of the ionic component of the polyelectrolyte at the top of the film.[132]

Very recently, Wang[133] and Kim[134] groups also reported the use of WSCPs as cathode interlayer to enhance the V_{oc} of polymer solar cells based on P3HT: PCBM. In order to prevent metal atoms penetrating into the active layer during thermal deposition process and reducing the leakage across the device, Zhao *et al.*[133] reported that the performance of P3HT: PCBM PSCs can be improved by depositing a thin layer of **P40** between the active layer and the cathode *via* spin coating from ethanol solution. Indeed, upon the incorporation of a thin layer of **P40** (5 nm), the shunt resistance increase from 31 kΩ cm^{-2} to 1.1 MΩ cm^{-2}, and the V_{oc} was enhanced up to 0.64 V (0.45 V for the control device). Furthermore, the fill factor was improved from 51% to 59%, leading to a PCE of 3.4% (*vs.* 2.0% for the control device). Na *et al.*[134] reported the use of a polyfluorene WSCP **P26** as cathode interlayer for PSCs. It was found that the insertion of **P26** (~3–6 nm) between the active layer (P3HT/PCBM) and Al cathode increased the PCE from 3.0% to 3.8%. It should be noticed that the V_{oc} of the device was found to be 0.68 V, 0.11 V enhancements as compared to the reference devices, which is independent on the thickness of the interlayer in range of 3–6 nm.

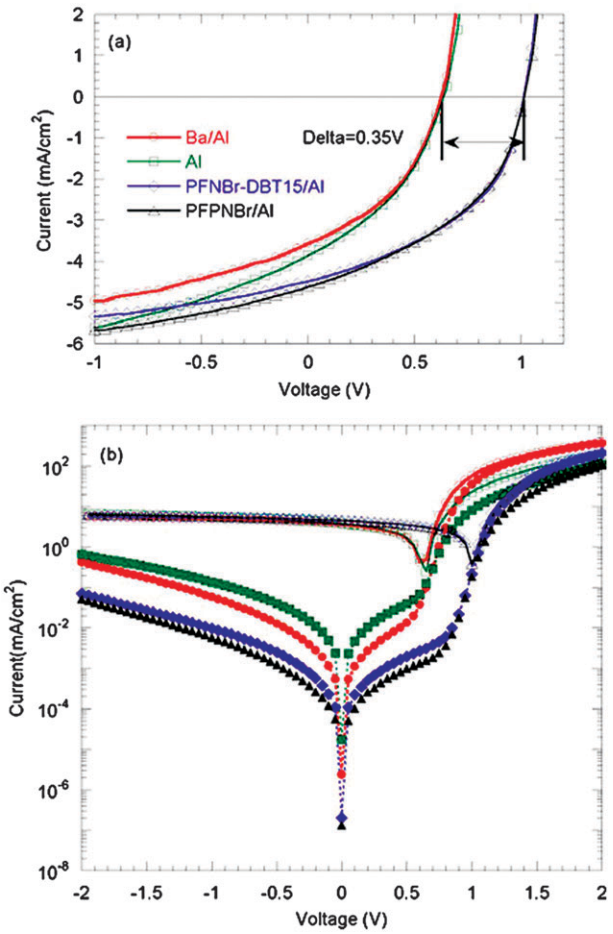

Fig. 14 (a) *J*–*V* characteristics of devices with a structure of ITO/PEDOT:PSS/PF-DBT35:PCBM (1 : 2, w/w) (70–80 nm)/various cathode under the illumination of an AM 1.5 G solar simulator (800 W m^{-2}) (b) A replot of Fig. 1a in double-log (open) together with the *J*–*V* characteristics of the devices in the dark (filled), Ba/Al cathode (circles), Al cathode (squares), PFNBr-DBT15/Al (diamonds) and PFPNBr/Al (triangles). Reproduced with permission from ref. 127. Copyright 2009 American Institute of Physics.

3.5 As buffer layer in OFETs

OFETs are of great interest in large-area, low-cost applications, such as OLEDs, organic complementary logic circuits and biosensors.[6,7] It is well known that the interface property between the gate insulator and the active layer plays an important role in the performance of OFETs. WSCPs have the potential of improving the interface contact between the gate insulator and the active layer due to their unique properties such as the strong polarity. Recently, Lan *et al.*[135] reported the using of WSCPs (**P41**, Scheme 9) with different polarities as interfacial modification layers in n-type OFETs with bottom gate configuration: Ta (gate)/Ta_2O_5 (gate insulator)/WSCPs (modification layer)/PTCDI (active layer)/Al (source and drain), where a typical n-type semiconductor *N*,*N*′-didodecyl-3,4,9,10-perylene tetracarboxylic diimides (PTCDI) was used as the active layer. **P41** was synthesized by using Pd-catalyzed Suzuki coupling of different monomers and its polarity can be tuned by the *x* to *y* ratios (the polarity reduces as the *x* to *y* ratios increase). Fig. 15 shows the transfer characteristics of

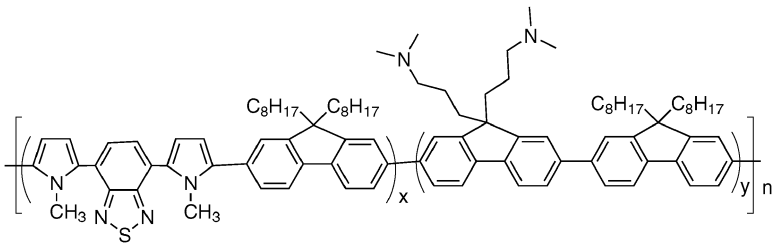

Scheme 9 Molecular structure of **P41**.

the OFET with and without WSCPs interfacial modification layers. The threshold voltages for the transistors with Ta_2O_5, Ta_2O_5/PFN (**P41**, $x = 0$, $y = 1$), Ta_2O_5/PFN-PBT1 (**P41**, x:$y = 1:49$), and Ta_2O_5/PFN-PBT5 (**P41**, x:$y = 1:9$) insulators were 12.5 V, 2.8 V, 4.8 V, and 6 V, respectively. Clearly, the threshold voltage decreased when Ta_2O_5 insulator was modified by the insertion of **P41** and increased as the x to y ratios increased. The change of threshold voltages was proved to be due to the self-assemble electric dipole field induced by the polar molecules. The mobility and the electrical stability increased with the increasing surface polarity of the gate insulator which was caused by the reduction of the interface-trap density. It is worth noting that the using of **P41** in p-type OFETs will depress the devices' performance (reducing mobility, and increasing threshold voltage), which implies that the direction of interface dipole moment is fixed and independent of the active materials. Since WSCPs can be dissolved in water and other polar solvents, they can modify most of the organic or inorganic gate insulators by spin-coating or printing methods. Thus, this work opens a new way in improving the performance of the OFETs.

4. Conclusions and outlook

This review provides an overview of the recent development of WSCPs as the interface modification layer in polymer opto-electronic devices. Due to the unique advantages of WSCPs in the application of optoelectronic devices, this novel research field received rapid development in a relative short period. A large number of WSCPs, with different main chain structures, side chain polar groups as well as couterions, have been developed and many fundamental studies have been performed to explore the function/property relationships of WSCPs. Most of the newly developed WSCPs were investigated for the application in PLEDs. Important breakthroughs have been made by using WSCPs as ETL in PLEDs that allow the use of stable high work-function metal cathodes (such as Al, Ag, Au *etc.*) for high efficiency devices. It was proposed that their distinguished electron injection properties were attributed to the dipole formation between the WSCPs ETL and metal cathode, while the ionic charge redistribution by the moving of the counterions were also found to play an important role on the excellent electron injection properties of conjugated polyelectrolytes based ETL. Nevertheless, high efficiency RGB and white-emitting PLEDs with WSCPs ETL and stable metal cathode were developed and showed comparable and even better performance than those of PLEDs with widely used active metal cathodes (such as Ca, Ba *etc.*). Most importantly, the WSCPs ETL materials offer the opportunities to realize polymer multilayer device structures. By using WSCPs as ETL and printable Ag paste as cathodes, the resulted all-printed PLEDs exhibited excellent device performance comparable to those reference devices with Ba/Al cathodes fabricated by thermal deposition. All these results indicate that the WSCPs can potentially exert the advantages of organic electronic to the most and will open a way to achieve all printable roll to roll polymer based organic electronic devices. The researches on application of WSCPs in PSCs and OFETs are not as extensively investigated as those on PLEDs in recent years. However, preliminary results have shown that the performance of both PSCs and OFETs' can be dramatically improved by using WSCPs interface modification layer. We note that the structural diversity of the used WSCPs is still limited and most of them are based on polyfluorene derivatives. Thus, with the experiences have obtained so far and with more varieties of WSCPs developed in future targeting specifically on the PSCs and OFETs, we expect further success of applications of WSCPs in these fields of organic electronics.

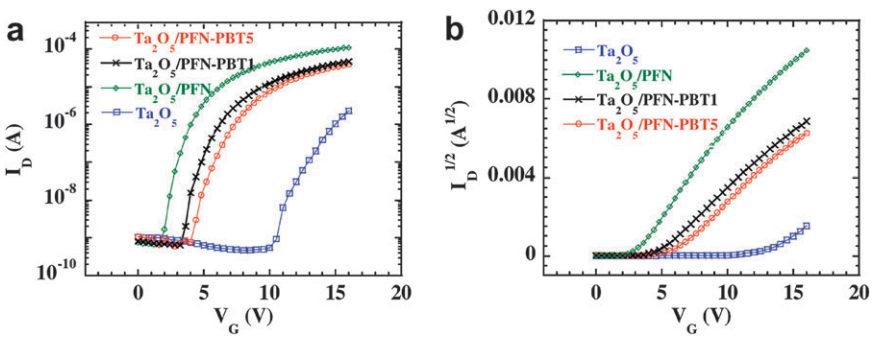

Fig. 15 Plots of (a) ID *vs.* VG, and (b) corresponding |ID|1/2 *vs.* VG for PTCDI OFFTs with insulators of Ta_2O_5, Ta_2O_5/PFN, Ta_2O_5/PFN-PBT1, and Ta_2O_5/PFN-PBT5 biased at VD = 16 V. Reproduced with permission from ref. 135 copyright 2005 Elsevier.

In summary, WSCPs are promising candidates for optoelectronic devices and offer the opportunities to fully exploit the potential of low-cost fabrication of organic optoelectronic devices with large area size.

Acknowledgements

The work was financially supported by the Natural Science Foundation of China (No. 50990065, 20904011, and 60906032) and the Ministry of Science and Technology, China (MOST) National Research Project (No. 2009CB623601).

References

1 J. H. Burroughes, D. D. C. Bradley, A. R. Brown, R. N. Marks, K. Mackay, R. H. Friend, P. L. Burn and A. B. Holmes, *Nature*, 1990, **347**, 539.
2 A. C. Grimsdale, K. L. Chan, R. E. Martin, P. G. Jokisz and A. B. Holmes, *Chem. Rev.*, 2009, **109**, 897 and the references therein.
3 G. Yu, J. Gao, J. C. Hummelen, F. Wudl and A. J. Heeger, *Science*, 1995, **270**, 1789.
4 S. Gnes, H. Neugebauer and N. S. Sariciftci, *Chem. Rev.*, 2007, **107**, 1324 and the references therein.
5 R. Kroon, M. Lenes, J. C. Hummelen, P. W. M. Blom and B. De Boer, *Polym. Rev.*, 2008, **48**, 531 and the references therein.
6 R. J. Li, H. X. Li, X. R. Zhou and W. P. Hu, *Progress In Chemistry*, 2007, **19**, 325 and the references therein.
7 S. Allard, M. Forster, B. Souharce, H. Thiem and U. Scherf, *Angew. Chem., Int. Ed.*, 2008, **47**, 4070.
8 M. R. Pinto and K. S. Schanze, *Synthesis*, 2002, 1293 and the references therein.
9 S. W. Thomas III, G. D. Joly and T. M. Swager, *Chem. Rev.*, 2007, **107**, 1339 and the references therein.
10 B. Liu and G. C. Bazan, *Chem. Mater.*, 2004, **16**, 4467 and the references therein.
11 C. W. Tang and S. A. VanSlyke, *Appl. Phys. Lett.*, 1987, **51**, 913.
12 A. P. Kulkarni, C. J. Tonzola, A. Babel and S. A. Jenekhe, *Chem. Mater.*, 2004, **16**, 4556 and the references therein.
13 G. Hughes and M. R. Bryce, *J. Mater. Chem.*, 2005, **15**, 94 and the references therein.
14 F. Huang, Y.-J. Cheng, Y. Zhang, M. S. Liu and A. K.-Y. Jen, *J. Mater. Chem.*, 2008, **18**, 4495 and the references therein.
15 H. Xiao, B. Leng and H. Tian, *Polymer*, 2005, **46**, 5707.
16 D. C. Müller, A. Falcou, N. Reckefuss, M. Rojahn, V. Wiederhirn, P. Rudati, H. Frohne, O. Nuyken, H. Becker and K. Meerholz, *Nature*, 2003, **421**, 829.
17 J. C. G. Veinot and T. J. Marks, *Acc. Chem. Res.*, 2005, **38**, 632 and the references therein.
18 F. Huang, H. B. Wu, J. B. Peng, W. Yang and Y. Cao, *Curr. Org. Chem.*, 2007, **11**, 1207 and the references therein.
19 C. V. Hoven, A. Garcia, G. C. Bazan and T.-Q. Nguyen, *Adv. Mater.*, 2008, **20**, 3793 and the references therein.
20 H. Jiang, P. Taranekar, J. R. Reynolds and K. S. Schanze, *Angew. Chem., Int. Ed.*, 2009, **48**, 4300 and the references therein.
21 D. W. Steuerman, A. Garcia, M. Dante, R. Q. Yang, J. P. Löfvander and T.-Q. Nguyen, *Adv. Mater.*, 2008, **20**, 528.
22 Z. Chen, C. Y. Jiang, Q. L. Niu, J. B. Peng and Y. Cao, *Org. Electron.*, 2008, **9**, 1002.
23 G. Decher, *Science*, 1997, **277**, 1232.
24 M. Ferreira and M. F. Rubner, *Macromolecules*, 1995, **28**, 7107.
25 A. O. Patil, Y. Ikenoue, F. Wudl and A. J. Heeger, *J. Am. Chem. Soc.*, 1987, **109**, 1858.
26 N. S. Sundaresan, S. Basak, M. Pomerantz and J. R. Reynolds, *J. Chem. Soc., Chem. Commun.*, 1987, 621.
27 J. R. Reynolds, N. S. Sundaresan, M. Pomerantz, S. Basak and C. K. Baker, *J. Electroanal. Chem.*, 1988, **250**, 355.
28 V. Cimrová, W. Schmidt, R. Rulkens, M. Schulze, W. Meyer and D. Neher, *Adv. Mater.*, 1996, **8**, 585.
29 A. F. Thünemann, *Adv. Mater.*, 1999, **11**, 127.
30 A. F. Thünemann and D. Ruppelt, *Langmuir*, 2001, **17**, 5098.
31 O. Onitsuka, A. C. Fou, M. Ferreira, B. R. Hsieh and M. F. Rubner, *J. Appl. Phys.*, 1996, **80**, 4067.
32 J. Tian, C. C. Wu, M. E. Thompson, J. C. Sturm, R. A. Register, M. J. Marsella and T. M. Swager, *Adv. Mater.*, 1995, **7**, 395.
33 S. Kim, J. Jackiw, E. Robinson, K. S. Schanze, J. R. Reynolds, J. Baur, M. F. Rubner and D. Boils, *Macromolecules*, 1998, **31**, 964.
34 J. W. Baur, S. Kim, P. B. Balanda, J. R. Reynolds and M. F. Rubner, *Adv. Mater.*, 1998, **10**, 1452.
35 J. M. Hodgkiss, G. Tu, S. Albert-Seifried, W. T. S. Huck and R. H. Friend, *J. Am. Chem. Soc.*, 2009, **131**, 8913.
36 F. Huang, H. B. Wu, D. L. Wang, W. Yang and Y. Cao, *Chem. Mater.*, 2004, **16**, 708.
37 H. B. Wu, F. Huang, Y. Q. Mo, W. Yang, D. L. Wang, J. B. Peng and Y. Cao, *Adv. Mater.*, 2004, **16**, 1826.
38 B. Liu, W.-L. Yu, Y.-H. Lai and W. Huang, *Macromolecules*, 2002, **35**, 4975.
39 Q. L. Fan, S. Lu, Y. H. Lai, X. Y. Hou and W. Huang, *Macromolecules*, 2003, **36**, 6976.
40 H.-H. Lu, C.-Y. Liu, T.-H. Jen, J.-L. Liao, H.-E. Tseng, C.-W. Huang, M.-C. Hung and S.-A. Chen, *Macromolecules*, 2005, **38**, 10829.
41 E. Aharon, A. Albo, M. Kalina and G. L. Frey, *Adv. Funct. Mater.*, 2006, **16**, 980.
42 D. Braun and A. J. Heeger, *Appl. Phys. Lett.*, 1991, **58**, 1982.
43 Y. Cao, G. Yu, I. D. Parker and A. J. Heeger, *J. Appl. Phys.*, 2000, **88**, 3618.
44 H. B. Wu, F. Huang, J. B. Peng and Y. Cao, *Synth. Met.*, 2005, **153**, 197.
45 H. B. Wu, F. Huang, Y. Q. Mo, W. Yang, J. B. Peng and Y. Cao, *J. SID.*, 2005, **13/2**, 123.
46 I. D. Parker, Y. Cao and C. Y. Yang, *J. Appl. Phys.*, 1999, **85**, 2441.
47 L. S. Hung, C. W. Tang and M. G. Mason, *Appl. Phys. Lett.*, 1997, **70**, 152.
48 P. Piromerium, H. Oh, Y. Shen, G. G. Malliaras, J. C. Scott and P. J. Brock, *Appl. Phys. Lett.*, 2000, **77**, 2403.
49 Y. Cao, G. Yu and A. J. Heeger, *Adv. Mater.*, 1998, **10**, 917.
50 H. B. Wu, F. Huang, J. B. Peng and Y. Cao, *Org. Electron.*, 2005, **6**, 118.
51 G. G. Malliaras, J. R. Salem, P. J. Brock and C. Scott, *Phys. Rev. B*, 1998, **58**, R13411.
52 C. J. Brabec, A. Cravino, D. Meissner, N. S. Sariciftci, F. Fromherz, M. T. Rispens, L. Sanchez and J. C. Hummelen, *Adv. Funct. Mater.*, 2001, **11**, 374.
53 H. Ishii, K. Sugiyama, E. Ito and K. Seki, *Adv. Mater.*, 1999, **11**, 605.
54 S. Braun, W. R. Salaneck and M. Fahlman, *Adv. Mater.*, 2009, **21**, 1450.
55 D. E. Aspnes, *Phys. Rev.*, 1966, **147**, 554.
56 G. Weiser, *Phys. Rev. B*, 1992, **45**, 14076.
57 M. Liess, S. Jeglinski, Z. V. Vardeny, M. Ozaki, K. Yoshino, Y. Ding and T. Barton, *Phys. Rev.*, 1997, **56**, 15712.
58 A. Horvata, H. Bassler and G. Weiser, *Phys. Status Solidi B*, 1992, **173**, 755.
59 T. W. Hagler, K. Pakbaz and A. J. Heeger, *Phys. Rev. B*, 1994, **49**, 10968.
60 I. H. Campbell, T. W. Hagler, D. L. Smith and J. P. Ferraris, *Phys. Rev. Lett.*, 1996, **76**, 1900.
61 I. H. Campbell, M. D. Joswick and I. D. Parker, *Appl. Phys. Lett.*, 1995, **67**, 3171.
62 T. M. Brown, R. H. Friend, S. Millard, D. J. Lacey, T. Butler, J. H. Burroughes and F. Cacialli, *J. Appl. Phys.*, 2003, **93**, 6159.
63 F. Huang, L. T. Hou, H. B. Wu, X. H. Wang, H. L. Shen, W. Cao, W. Yang and Y. Cao, *J. Am. Chem. Soc.*, 2004, **126**, 9845.
64 F. Huang, L. T. Hou, H. L. Shen, J. X. Jiang, F. Wang, H. Y. Zhen, W. Cao, W. Yang and Y. Cao, *J. Mater. Chem.*, 2005, **15**, 2499.
65 H. L. Shen, F. Huang, L. T. Hou, H. B. Wu, W. Cao, W. Yang and Y. Cao, *Synth. Met.*, 2005, **152**, 257.
66 F. Huang, L. T. Hou, H. L. Shen, R. Q. Yang, Q. Hou and Y. Cao, *J. Polym. Sci., Part A: Polym. Chem.*, 2006, **44**, 2521.
67 F. Huang, L. T. Hou, W. Shi, W. Cao, Q. Hou, W. Yang and Y. Cao, *Eur. Polym. J.*, 2006, **42**, 2320.
68 L. T. Hou, F. Huang, J. B. Peng, H. B. Wu, S. S. Wen, Y. Q. Mo and Y. Cao, *Thin Solid Films*, 2006, **515**, 2632.
69 L. Wang, B. Liang, F. Huang, J. B. Peng and Y. Cao, *Appl. Phys. Lett.*, 2006, **89**, 151115.

70 M. A. Baldo, D. F. O'Brien, Y. You, A. Shoustikov, S. Sibley, M. E. Thompson and S. R. Forrest, *Nature*, 1998, **395**, 151.
71 Y. Zhang, Y. H. Xu, Q. L. Niu, J. B. Peng, W. Yang, X. H. Zhu and Y. Cao, *J. Mater. Chem.*, 2007, **17**, 992.
72 Y. Zhang, Y. Xiong, Y. H. Sun, X. H. Zhu, J. B. Peng and Y. Cao, *Polymer*, 2007, **48**, 3468.
73 Y. Zhang, Y. Xiong, R. S. Liu, J. B. Peng and Y. Cao, *Acta Chimica Sinica*, 2007, **24**, 2929.
74 Y. Zhang, Z. Huang, W. J. Zeng and Y. Cao, *Polymer*, 2008, **49**, 1211.
75 L. Ying, Y. H. Xu, W. Yang, L. Wang, H. B. Wu and Y. Cao, *Org. Electron.*, 2009, **10**, 42.
76 W. L. Ma, P. K. Iyer, X. Gong, B. Liu, D. Moses, G. C. Bazan and A. J. Heeger, *Adv. Mater.*, 2005, **17**, 24.
77 S.-H. Oh, S.-I. Na, Y.-C. Nah, D. Vak, S.-S. Kim and D.-Y. Kim, *Org. Electron.*, 2007, **8**, 773.
78 D. Vak, S.-H. Oh and D.-Y. Kim, *Appl. Phys. Lett.*, 2009, **94**, 243305.
79 S.-H. Oh, D. Vak, S.-I. Na, T.-W. Lee and D.-Y. Kim, *Adv. Mater.*, 2008, **20**, 1624.
80 Q. Pei, G. Yu, C. Zhang, Y. Yang and A. J. Heeger, *Science*, 1995, **269**, 1086.
81 J. Morgado, R. H. Friend, F. Cacialli, B. S. Chuah, H. Rost, S. C. Moratti and A. B. Holmes, *Synth. Met.*, 2001, **122**, 111.
82 H. P. Wang, P. Lu, B. L. Wang, S. Qiu, M. R. Liu, M. Hanif, G. Cheng, S. Y. Liu and Y. G. Ma, *Macromol. Rapid Commun.*, 2007, **28**, 1645.
83 R. Q. Yang, A. Garcia, D. Korystov, A. Mikhailovsky, G. C. Bazan and T.-Q. Nguyen, *J. Am. Chem. Soc.*, 2006, **128**, 16532.
84 R. Q. Yang, H. B. Wu, Y. Cao and G. C. Bazan, *J. Am. Chem. Soc.*, 2006, **128**, 14422.
85 C. Hoven, R. Q. Yang, A. Garcia, A. J. Heeger, T.-Q. Nguyen and G. C. Bazan, *J. Am. Chem. Soc.*, 2007, **129**, 10976.
86 D. J. Pinner, R. H. Friend and N. Tesslera, *J. Appl. Phys.*, 1999, **86**, 5116.
87 P. W. M. Blom and M. C. J. M. Vissenberg, *Phys. Rev. Lett.*, 1998, **80**, 3819.
88 Q. B. Pei, Y. Yang, G. Yu, C. Zhang and A. J. Heeger, *J. Am. Chem. Soc.*, 1996, **118**, 3922.
89 J. C. deMello, N. Tessler, S. C. Graham and R. H. Friend, *Phys. Rev. B*, 1998, **57**, 12951.
90 C. V. Hoven, R. Q. Yang, A. Garcia, V. Crockett, A. J. Heeger, G. C. Bazan and T.-Q. Nguyen, *Proc. Natl. Acad. Sci. U. S. A.*, 2008, **105**, 12730.
91 C. V. Hoven, J. Peet, A. Milhailovsky and T.-Q. Nguyen, *Appl. Phys. Lett.*, 2009, **94**, 033301.
92 F. Huang, Y. H. Niu, Y. Zhang, J. W. Ka, M. S. Liu and A. K.-Y. Jen, *Adv. Mater.*, 2007, **19**, 2010.
93 F. Huang, Y. Zhang, M. S. Liu and A. K.-Y. Jen, *Adv. Funct. Mater.*, 2009, **19**, 2457.
94 F. Huang, Y. Zhang, M. S. Liu, Y.-J. Cheng and A. K.-Y. Jen, *Adv. Funct. Mater.*, 2007, **17**, 3808.
95 F. Huang, P. I. Shih, M. S. Liu, C. F. Shu and A. K.-Y. Jen, *Appl. Phys. Lett.*, 2008, **93**, 243302.
96 Y. H. Niu, H. Ma, Q. M. Xu and A. K.-Y. Jen, *Appl. Phys. Lett.*, 2005, **86**, 083504.
97 Y. H. Niu, A. K.-Y. Jen and C. F. Shu, *J. Phys. Chem. B*, 2006, **110**, 6010.
98 T. H. Lee, J. C. A. Huang, G. L. Pakhomov, T. F. Guo, T. C. Wen, Y. S. Huang, C. C. Tsou, C. T. Chung, Y. C. Lin and Y. J. Hsu, *Adv. Funct. Mater.*, 2008, **18**, 3036.
99 X. H. Yang and D. Neher, *Appl. Phys. Lett.*, 2004, **84**, 2476.
100 F. Huang, Y. H. Niu, M. S. Liu, X. H. Zhou, Y. Q. Tian and A. K.-Y. Jen, *Appl. Phys. Lett.*, 2006, **89**, 081104.
101 A. J. Campbell, D. D. C. Bradley and H. Antoniadis, *Appl. Phys. Lett.*, 2001, **79**, 2133.
102 C. L. Donley, J. Zaumseil, J. W. Andreasen, M. M. Nielsen, H. Sirringhaus, R. H. Friend and J. S. Kim, *J. Am. Chem. Soc.*, 2005, **127**, 12890.
103 J. Luo, J. B. Peng, Y. Cao and Q. Hou, *Appl. Phys. Lett.*, 2005, **87**, 261103.
104 T.-W. Lee, T. Noh, B.-K. Choi, M.-S. Kim, D. W. Shin and J. Kido, *Appl. Phys. Lett.*, 2008, **92**, 043301.
105 K. Roy Choudhury, J.-h. Yoon and F. So, *Adv. Mater.*, 2008, **20**, 1456.
106 F. Huang, X. H. Wang, D. L. Wang, W. Yang and Y. Cao, *Polymer*, 2005, **46**, 12010.
107 A. Garcia, R. Q. Yang, Y. Jin, B. Walker and T.-Q. Nguyen, *Appl. Phys. Lett.*, 2007, **91**, 153502.
108 Y. Jin, G. C. Bazan, A. J. Heeger, J. Y. Kim and K. Lee, *Appl. Phys. Lett.*, 2008, **93**, 123304.
109 G. Zhou, G. Qian, L. Ma, Y. X. Cheng, Z. Y. Xie, L. X. Wang, X. B. Jing and F. S. Wang, *Macromolecules*, 2005, **38**, 5416.
110 G. Zhou, Y. H. Geng, Y. X. Cheng, Z. Y. Xie, L. X. Wang, X. B. Jing and F. S. Wang, *Appl. Phys. Lett.*, 2006, **89**, 233501.
111 H. B. Wu, L. Ying, W. Yang and Y. Cao, *Chem. Soc. Rev.*, 2009, **38**, 3391.
112 B. W. D'Andrade and S. R. Forrest, *Adv. Mater.*, 2004, **16**, 1585.
113 X. Gong, S. Wang, D. Moses, G. C. Bazan and A. J. Heeger, *Adv. Mater.*, 2005, **17**, 2053.
114 D. An, J. H. Zou, H. B. Wu, J. B. Peng, W. Yang and Y. Cao, *Org. Electron.*, 2009, **10**, 299.
115 Y. H. Xu, R. Q. Yang, J. B. Peng, A. A. Mikhailovsky, Y. Cao, T.-Q. Nguyen and G. C. Bazan, *Adv. Mater.*, 2009, **21**, 584.
116 Y. Zhang, F. Huang, A. K.-Y. Jen and Y. Chi, *Appl. Phys. Lett.*, 2008, **92**, 063303.
117 Y. Zhang, F. Huang, Y. Chi and A. K.-Y. Jen, *Adv. Mater.*, 2008, **20**, 1565.
118 F. Huang, P.-I. Shih, C.-F. Shu, Y. Chi and A. K.-Y. Jen, *Adv. Mater.*, 2009, **21**, 361.
119 X. D. Niu, C. J. Qin, B. H. Zhang, J. W. Yang, Z. Y. Xie, Y. X. Cheng and L. X. Wang, *Appl. Phys. Lett.*, 2007, **90**, 203513.
120 Y. R. Sun, N. C. Giebink, H. Kanno, B. W. Ma, M. E. Thompson and S. R. Forrest, *Nature*, 2006, **440**, 908.
121 L. T. Hou, F. Huang, W. J. Zeng, J. B. Peng and Y. Cao, *Appl. Phys. Lett.*, 2005, **87**, 153509.
122 L. T. Hou, F. Huang, Y. Cao and P. Y. Liu, *Progress in Chemistry*, 2007, **19**, 1681.
123 M. Stewart, R. S. Howell, L. Pires and M. K. Hatalis, *IEEE Trans. Electron Devices*, 2001, **48**, 845.
124 W. J. Zeng, H. B. Wu, C. Zhang, F. Huang, J. B. Peng, W. Yang and Y. Cao, *Adv. Mater.*, 2007, **19**, 810.
125 S. H. Park, A. Roy, S. Beaupre, S. Cho, N. Coates, J. S. Moon, D. Moses, M. Leclerc, K. G. Lee and A. J. Heeger, *Nat. Photonics*, 2009, **3**, 297.
126 Y. Y. Liang, D. Q. Feng, Y. Wu, S.-T. Tsai, G. Li, C. Ray and L. P. Yu, *J. Am. Chem. Soc.*, 2009, **131**, 7792.
127 J. Luo, H. B. Wu, C. He, A. Y. Li, W. Yang and Y. Cao, *Appl. Phys. Lett.*, 2009, **95**, 043301.
128 Q. Hou, Y. S. Xu, W. Yang, M. Yuan, J. B. Peng and Y. Cao, *J. Mater. Chem.*, 2002, **12**, 2887.
129 Q. M. Zhou, Q. Hou, L. P. Zheng, X. Y. Deng, G. Yu and Y. Cao, *Appl. Phys. Lett.*, 2004, **84**, 1653.
130 M. C. Scharber, D. Mühlbacher, M. Koppe, P. Denk, C. Waldauf, A. J. Heeger and C. J. Brabec, *Adv. Mater.*, 2006, **18**, 789.
131 F. Wang, J. Luo, K. X. Yang, J. W. Chen, F. Huang and Yong Cao, *Macromolecules*, 2005, **38**, 2253.
132 J. Park, R. Q. Yang, C. V. Hoven, A. Garcia, D. A. Fischer, T. Q. Nguyen, G. C. Bazan and D. M. DeLongchamp, *Adv. Mater.*, 2008, **20**, 2491.
133 Y. Zhao, Z. Y. Xie, C. J. Qin, Y. Qu, Y. H. Geng and L. X. Wang, *Sol. Energy Mater. Sol. Cells*, 2009, **93**, 604.
134 S.-I. Na, S.-H. Oh, S.-S. Kim and D.-Y. Kim, *Org. Electron.*, 2009, **10**, 496.
135 L. Lan, J. Peng, M. Sun, J. Zhou, J. Zou, J. Wang and Y. Cao, *Org. Electron.*, 2009, **10**, 346.